AD-A064 077 AIR FORCE INST OF TECH WRIGHT-PATTERSON AFB OHIO F/G 20/8
PROJECTILE ENERGY DEPENDENCE OF ALUMINUM AND SILICON KA X-RAY S--ETC(U)
AUG 78 B I SONOBE
UNCLASSIFIED AFIT-CI-79-90T NL

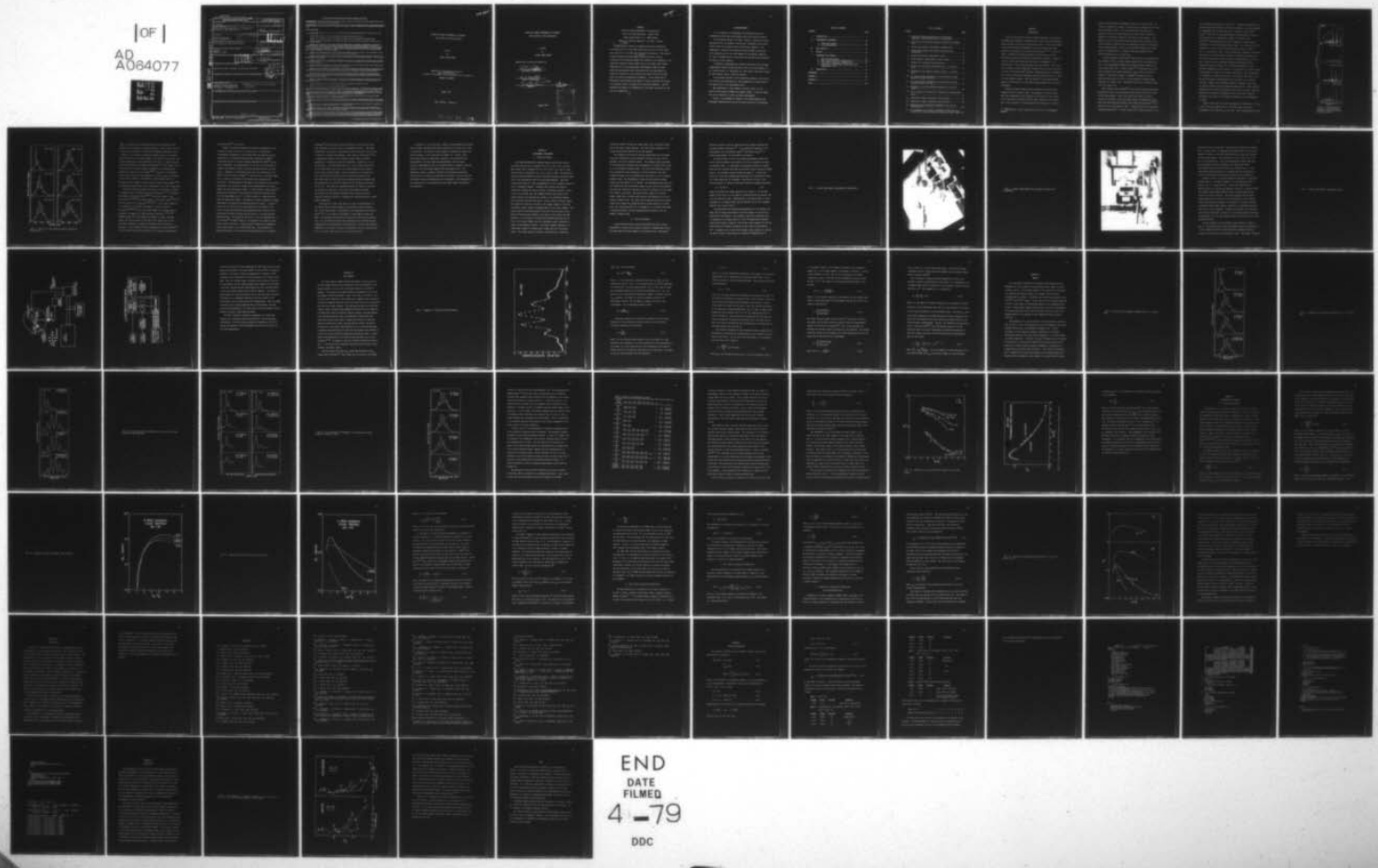

END
DATE FILMED
4-79
DDC

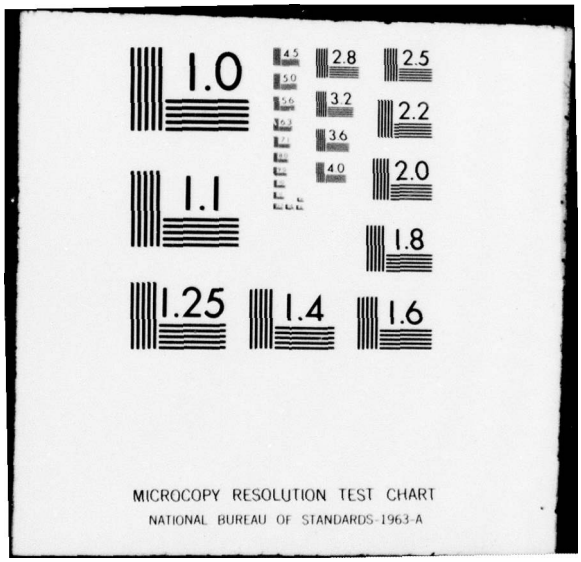
1.0
1.1
1.25
1.4
1.6
1.8
2.0
2.2
2.5
2.8
3.2
3.6
4.0
4.5
5.0
5.6
6.3
7.1
8.0
9.0
MICROCOPY RESOLUTION TEST CHART
NATIONAL BUREAU OF STANDARDS-1963-A

UNCLASSIFIED

SECURITY CLASSIFICATION OF THIS PAGE *(When Data Entered)*

REPORT DOCUMENTATION PAGE

READ INSTRUCTIONS BEFORE COMPLETING FORM

1. REPORT NUMBER: CI 79-90T
2. GOVT ACCESSION NO.
3. RECIPIENT'S CATALOG NUMBER

4. TITLE *(and Subtitle)*: Projectile Energy Dependence of Aluminum and Silicon Ka X-Ray Satellites
5. TYPE OF REPORT & PERIOD COVERED: Thesis
6. PERFORMING ORG. REPORT NUMBER

7. AUTHOR(s): Blake Isamu Sonobe
8. CONTRACT OR GRANT NUMBER(s): AFIT-CI-79-90T

9. PERFORMING ORGANIZATION NAME AND ADDRESS: AFIT Student at Texas A&M University
10. PROGRAM ELEMENT, PROJECT, AREA & WORK UNIT NUMBERS: Master's thesis

11. CONTROLLING OFFICE NAME AND ADDRESS: AFIT/CI, WPAFB OH 45433
12. REPORT DATE: August 1978
13. NUMBER OF PAGES: 80 (88p.)

14. MONITORING AGENCY NAME & ADDRESS *(if different from Controlling Office)*
15. SECURITY CLASS. *(of this report)*: Unclassified
15a. DECLASSIFICATION/DOWNGRADING SCHEDULE

LEVEL II

16. DISTRIBUTION STATEMENT *(of this Report)*

Approved for Public Release, Distribution Unlimited

DDC RECEIVED FEB 1 1979 C

17. DISTRIBUTION STATEMENT *(of the abstract entered in Block 20, if different from Report)*

18. SUPPLEMENTARY NOTES

JOSEPH P. HIPPS, Major, USAF
Director of Information, AFIT

APPROVED FOR PUBLIC RELEASE AFR 190-17.
1-24-79

19. KEY WORDS *(Continue on reverse side if necessary and identify by block number)*

20. ABSTRACT *(Continue on reverse side if necessary and identify by block number)*

012 200

DD FORM 1 JAN 73 1473 EDITION OF 1 NOV 65 IS OBSOLETE

UNCLASSIFIED

SECURITY CLASSIFICATION OF THIS PAGE *(When Data Entered)*

DDC FILE COPY AD A064077

INSTRUCTIONS FOR PREPARATION OF REPORT DOCUMENTATION PAGE

RESPONSIBILITY. The controlling DoD office will be responsible for completion of the Report Documentation Page, DD Form 1473, in all technical reports prepared by or for DoD organizations.

CLASSIFICATION. Since this Report Documentation Page, DD Form 1473, is used in preparing announcements, bibliographies, and data banks, it should be unclassified if possible. If a classification is required, identify the classified items on the page by the appropriate symbol.

COMPLETION GUIDE

General. Make Blocks 1, 4, 5, 6, 7, 11, 13, 15, and 16 agree with the corresponding information on the report cover. Leave Blocks 2 and 3 blank.

Block 1. Report Number. Enter the unique alphanumeric report number shown on the cover.

Block 2. Government Accession No. Leave Blank. This space is for use by the Defense Documentation Center.

Block 3. Recipient's Catalog Number. Leave blank. This space is for the use of the report recipient to assist in future retrieval of the document.

Block 4. Title and Subtitle. Enter the title in all capital letters exactly as it appears on the publication. Titles should be unclassified whenever possible. Write out the English equivalent for Greek letters and mathematical symbols in the title *(see "Abstracting Scientific and Technical Reports of Defense-sponsored RDT/E," AD-667 000)*. If the report has a subtitle, this subtitle should follow the main title, be separated by a comma or semicolon if appropriate, and be initially capitalized. If a publication has a title in a foreign language, translate the title into English and follow the English translation with the title in the original language. Make every effort to simplify the title before publication.

Block 5. Type of Report and Period Covered. Indicate here whether report is interim, final, etc., and, if applicable, inclusive dates of period covered, such as the life of a contract covered in a final contractor report.

Block 6. Performing Organization Report Number. Only numbers other than the official report number shown in Block 1, such as series numbers for in-house reports or a contractor/grantee number assigned by him, will be placed in this space. If no such numbers are used, leave this space blank.

Block 7. Author*(s)*. Include corresponding information from the report cover. Give the name*(s)* of the author*(s)* in conventional order *(for example, John R. Doe or, if author prefers, J. Robert Doe)*. In addition, list the affiliation of an author if it differs from that of the performing organization.

Block 8. Contract or Grant Number(s). For a contractor or grantee report, enter the complete contract or grant number*(s)* under which the work reported was accomplished. Leave blank in in-house reports.

Block 9. Performing Organization Name and Address. For in-house reports enter the name and address, including office symbol, of the performing activity. For contractor or grantee reports enter the name and address of the contractor or grantee who prepared the report and identify the appropriate corporate division, school, laboratory, etc., of the author. List city, state, and ZIP Code.

Block 10. Program Element, Project, Task Area, and Work Unit Numbers. Enter here the number code from the applicable Department of Defense form, such as the DD Form 1498, "Research and Technology Work Unit Summary" or the DD Form 1634, "Research and Development Planning Summary," which identifies the program element, project, task area, and work unit or equivalent under which the work was authorized.

Block 11. Controlling Office Name and Address. Enter the full, official name and address, including office symbol, of the controlling office. *(Equates to funding/sponsoring agency. For definition see DoD Directive 5200.20, "Distribution Statements on Technical Documents.")*

Block 12. Report Date. Enter here the day, month, and year or month and year as shown on the cover.

Block 13. Number of Pages. Enter the total number of pages.

Block 14. Monitoring Agency Name and Address *(if different from Controlling Office)*. For use when the controlling or funding office does not directly administer a project, contract, or grant, but delegates the administrative responsibility to another organization.

Blocks 15 & 15a. Security Classification of the Report: Declassification/Downgrading Schedule of the Report. Enter in 15 the highest classification of the report. If appropriate, enter in 15a the declassification/downgrading schedule of the report, using the abbreviations for declassification/downgrading schedules listed in paragraph 4-207 of DoD 5200.1-R.

Block 16. Distribution Statement of the Report. Insert here the applicable distribution statement of the report from DoD Directive 5200.20, "Distribution Statements on Technical Documents."

Block 17. Distribution Statement *(of the abstract entered in Block 20, if different from the distribution statement of the report)*. Insert here the applicable distribution statement of the abstract from DoD Directive 5200.20, "Distribution Statements on Technical Documents."

Block 18. Supplementary Notes. Enter information not included elsewhere but useful, such as: Prepared in cooperation with . . . Translation of *(or by)* . . . Presented at conference of . . . To be published in . . .

Block 19. Key Words. Select terms or short phrases that identify the principal subjects covered in the report, and are sufficiently specific and precise to be used as index entries for cataloging, conforming to standard terminology. The DoD "Thesaurus of Engineering and Scientific Terms" *(TEST)*, AD-672 000, can be helpful.

Block 20. Abstract. The abstract should be a brief *(not to exceed 200 words)* factual summary of the most significant information contained in the report. If possible, the abstract of a classified report should be unclassified and the abstract to an unclassified report should consist of publicly- releasable information. If the report contains a significant bibliography or literature survey, mention it here. For information on preparing abstracts see "Abstracting Scientific and Technical Reports of Defense-Sponsored RDT&E," AD-667 000.

☆ U.S. GOVERNMENT PRINTING OFFICE : 1973—729-091/1431 3-1

PROJECTILE ENERGY DEPENDENCE OF ALUMINUM AND SILICON Kα X-RAY SATELLITES

A Thesis

by

BLAKE ISAMU SONOBE

Submitted to the Graduate College of
Texas A&M University
in partial fulfillment of the requirement for the degree of

MASTER OF SCIENCE

August 1978

Major Subject: Chemistry

PROJECTILE ENERGY DEPENDENCE OF ALUMINUM AND SILICON Kα X-RAY SATELLITES

A Thesis

by

BLAKE ISAMU SONOBE

Approved as to style and content by:

R. L. Watson
(Chairman of Committee)

G. E. Martell
(Head of Department)

Y.N. ZANG
(Member)

J. H Reading
(Member)

August 1978

ABSTRACT

Projectile Energy Dependence of Aluminum and Silicon Kα X-Ray Satellites. (August 1978)

Blake Isamu Sonobe, B. S., USAF Academy

Chairman of Advisory Committee: Dr. Rand L. Watson

The Kα satellite spectra of aluminum and silicon produced by collisions with 5.4 to 40.6 MeV helium ions, 12.0 to 74.1 MeV carbon ions, and 23.4 to 117.0 MeV neon ions have been measured. The apparent average L-vacancy fractions (p_L) determined from the relative intensities of the satellite peaks were observed to be dependent on the projectile energy and atomic number and on the target atomic number. Comparisons of the binary-encounter approximation (BEA) and semi-classical approximation (SCA) predictions with the experimental p_L values as a function of the projectile-to-L-shell electron velocity ratio for helium on aluminum are presented. It was found that the BEA greatly over-predicted the degree of L-shell ionization and failed to accurately predict the shape of the velocity dependence. The SCA predicted the shape of the dependence at the higher velocities but was too low in magnitude.

ACKNOWLEDGEMENTS

It is a pleasure to acknowledge the following persons and organizations whose advice and support made this research possible.

To my research advisor, Dr. Rand L. Watson, I express my sincere appreciation for his guidance, instruction, friendship, and patience without which this research could not have been completed. His commitment to students and research has been extremely motivating. I am also appreciative of the other members of my graduate committee, Dr. John F. Reading and Dr. Yi-Noo Tang, who provided much inspiration and advice in this research.

I thankfully acknowledge the technical assistance and late-night companionship during the many cyclotron runs of the other members of our research group, Dr. Tang Chiao, Mr. Fred Jenson, Miss Alice Leeper, Mr. Mark Michael, and Mr. Jefferey Sjurseth.

I am sincerely grateful to the operations personnel at the Cyclotron Institute and especially Mr. Jack Hernandez who prepared many of the targets used in the experimental work.

Most importantly, I give thanks to my wife, Janie, for her affection and support throughout my degree program. A special thanks also to our families for their continued encouragement.

Finally, I acknowledge the support of the Energy Research and Development Administration and the Air Force Institute of Technology.

TABLE OF CONTENTS

LIST OF FIGURES

CHAPTER I

INTRODUCTION

Since the discovery of x-rays in 1895 by Roentgen,[1] who observed this mysterious radiation from radioactive sources, many investigations have been made to produce and characterize x-rays. In the early 1900's x-rays were produced by bombardment of various targets with alpha particles from radioactive sources and by electrons.[2-12] In the late 1920's, Gerthsen[13] performed experiments using protons and alpha particles to study the production of inner-shell vacancies. Coates,[14] in 1934, found x-rays resulting from heavy ion bombardment to be characteristic of the atoms from which they were emitted. One of the early studies of x-rays produced by charged particles from an accelerator came in 1953 when Lewis[15] observed tremendous amounts of characteristic x-rays from proton bombardment (energies ranging from 1 to 3 MeV) on thick tantalum targets. Huus and Zupancic[16] also observed large amounts of characteristic x-rays while studying gamma rays from proton bombardment.

Energetic charged particles from accelerators have since been frequently used to produce x-rays. The passage of a heavy charged particle through matter often results in the ejection of one or more of the inner-shell electrons from the atomic orbitals of the target atom. This ionization is characterized by the emission of x-rays or

---

The citations in this thesis follow the style of the Physical Review A.

Auger electrons during the subsequent decay of the excited atom. Kα x-rays are emitted as a result of a 2p→1s electron transition in an atom with one K-shell vacancy. Kα x-ray satellites result when this transition occurs in an atom having one or more L-shell vacancies in addition to the K-shell vacancy at the time of x-ray emission. The absence of one or more L-shell electrons reduces the screening of the nuclear potential experienced by the remaining electrons and increases their binding energies. The Kα x-ray transition energy is increased above its characteristic or "normal" value and produces Kα x-ray satellite peaks in the x-ray spectrum.

In 1916, Siegbahn and Stenstrom[9] first noticed x-ray satellites as low intensity lines at slightly higher energies than the normal $K\alpha_{1,2}$ line. Their measurements extended from sodium (atomic number 11) to zinc (atomic number 30). In 1921, Wentzel[17,18] postulated that these lines originated from atoms having one or more L-shell vacancies in addition to the K-shell vacancy. Richtmyer[19] proposed that the satellite lines were the result of two simultaneous electron jumps resulting in a single x-ray. The Wentzel theory has since been proven to be the correct one.

More recently, many authors[20-24] have studied multiple inner-shell ionization by heavy ion projectiles by observing the shifts of the Kα and Kβ x-ray energies. They noted that as the degree of L-shell ionization increased, the energy shifts became correspondingly larger. High resolution Bragg spectrometers have enabled investigators[25-28] to resolve the Kα x-ray satellite lines. Various theoretical calculations (Herman-Skillman HFS,[29] C. Froese Fischer HF,[30] Veigele program,[31] etc.)

have confirmed the identity of these lines. McCrary and Richard[27] also observed multiplet structure in the Kα x-ray spectra of silicon produced by bombardment with 30 MeV oxygen ions. As early as 1929, Ray,[32] Langer,[33] and Wolfe,[34] using spectroscopic interpretations, predicted that satellites were composed of a number of multiplet lines. Bhalla[35,36] and Kauffman et al.[37] have attempted to assign relative intensities to the various spectroscopic terms. An illustration of the complexity of the Kα x-ray satellite spectrum of neon is shown in Fig. 1. The spectra in Fig. 1 were constructed by assuming a statistical population of the spectroscopic terms and a binomial distribution for the relative population of the electronic configurations ($p_L = 0.375$), and by using the x-ray transition energies and multiplet partial fluorescence yields of Bhalla.[35] The relative intensities of the multiplet components for the various 2s- and 2p-orbital (L-shell) vacancy configurations are given in the lower three spectra. The top spectrum is a composite of these three spectra. The notation (KL^n) used in the top spectrum denotes configurations with one K-shell and n L-shell vacancies. Despite the overlapping multiplet components, most lines are grouped together such that individual peaks result. These multiplet components and the reduced screening of the nuclear potential resulting from M-shell vacancies in addition to the K- and L-shell vacancies existing at the time of x-ray emission contribute to the broadening of the peaks.

Typical silicon Kα x-ray spectra produced by 2 MeV/amu He, C, O, Ne, S, and Ar ions are shown in Fig. 2. The first peak on the left corresponds to the normal $K\alpha_{1,2}$ x-ray line. Each succeeding peak to the

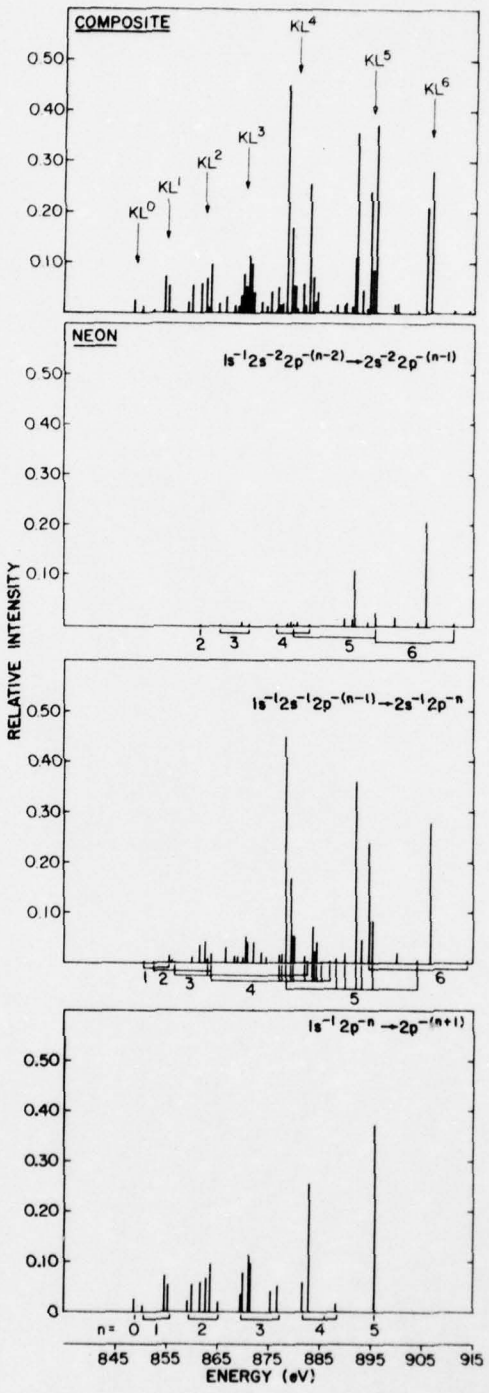

FIG. 1. Predicted relative intensities of the multiplet components comprising the neon Kα x-ray spectrum.

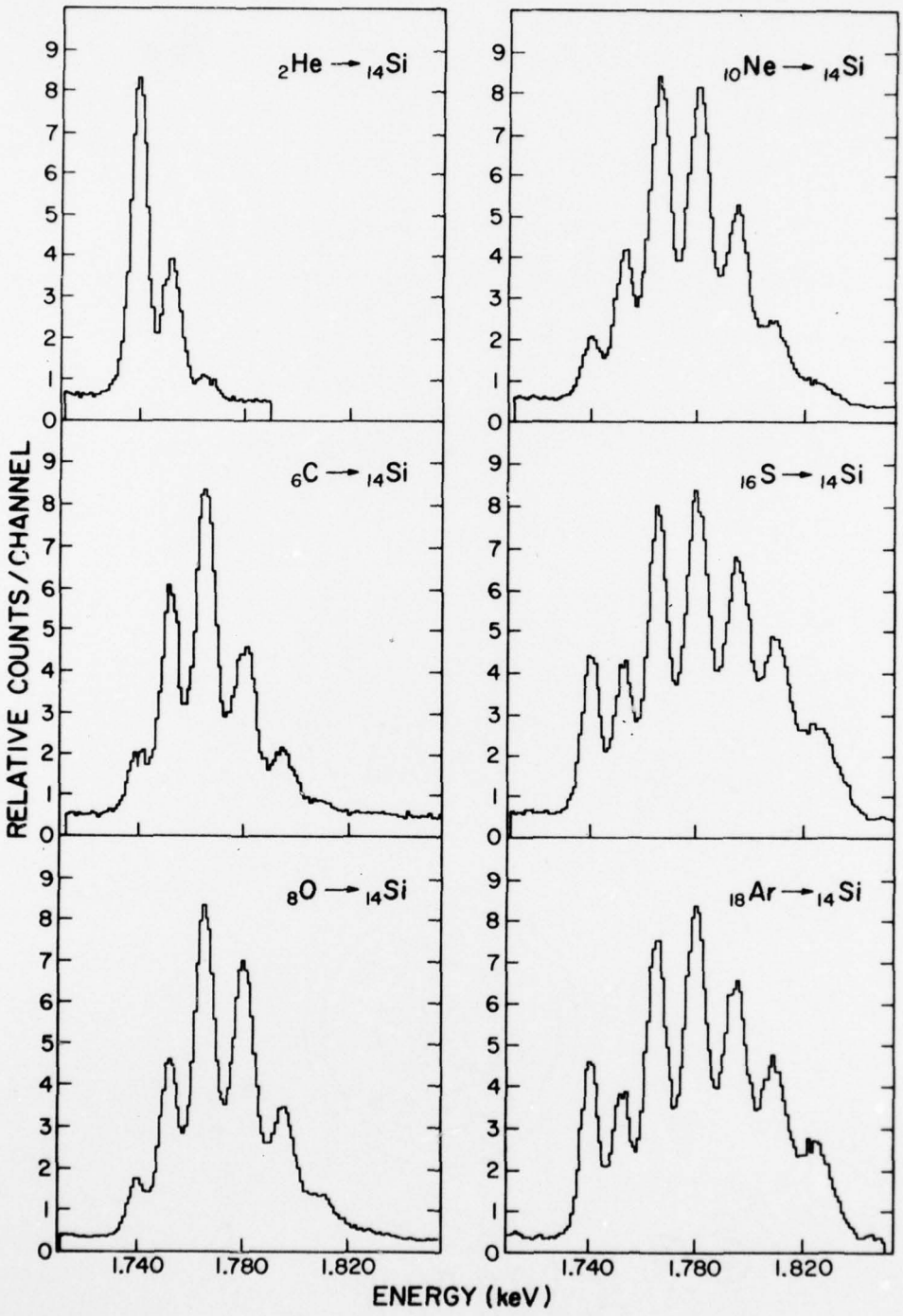

FIG. 2. Silicon Kα x-ray satellite spectra produced by 2 MeV/amu ions.

right is a satellite line associated with Kα x-ray emission in the presence of one through six L-shell vacancies. The KL^7 peak is cut off in the S and Ar spectra by the silicon K absorption edge which occurs at 1838 eV. The intensity distribution rapidly shifts to the higher order satellites as the atomic number of the projectile increases. The relative intensities of the satellites in the He, C, O, and Ne spectra can be well described by binomial distributions.[38] This appears to be a characteristic of satellite spectra produced by ions having atomic numbers less than that of the target.[39,40] Departures from binomial distributions caused by the enhancement of the $K\alpha_{1,2}$ peak are observed in the S and Ar spectra. This feature is only observed when the projectile atomic number is greater than the target atomic number.[39,41] The mechanisms contributing to this enhancement are not fully understood.

Detailed studies have shown that the Kα x-ray satellite structure is dependent upon the charge state of the projectile,[42,43] the chemical environment of the target atom,[39,44-47] the atomic number of the projectile,[40,42,48-52] the atomic number of the target atom,[40,49,51,53] and the energy of the projectile.[49,52,54-56] As the atomic number of the projectile is increased, the degree of L-shell ionization increases,[40,42,48-52] and as the atomic number of the target atom is increased, the degree of L-shell ionization decreases.[40,49,51,53] Kauffman et al.[42,43] have observed in studies of carbon, nitrogen, oxygen, and fluorine ions on neon that as the charge state of the projectile increases, the degree of multiple L-shell ionization increases. In the chemical effects investigations, energy shifts[44-46] of the Kα and Kβ structures and shifts in the relative intensities of

the satellites[39,47] were noted.

Despite the numerous studies of Kα satellite dependence on the projectile energy carried out in recent years, a comprehensive investigation encompassing a wide energy range and compared with the predictions of an improved binary-encounter approximation (BEA)[57] formulation and with the semi-classical approximation (SCA)[58] has not been accomplished. The applicability of the SCA to the prediction of single K- and multiple L-shell ionization probabilities has not been tested. Comparison of experimental data with the predictions of the BEA[57] was done by Olsen and Moore.[56] They used 24.0 to 48.0 MeV oxygen ions to study the calcium Kα x-ray satellite and hypersatellite structures. The BEA predicted the shape of the ionization cross section dependence on the projectile energy but was approximately 50 percent higher than the experimental values. In other studies, Knudson et al.[54] measured the aluminum Kα x-ray yields from collisions with neon ions over an energy range from 1.5 to 15 MeV, however, no comparisons were made with theoretical models. The degree of L-shell ionization in these measurements increased with increasing projectile energy. Li et al.[49] noted that the fraction of Kβ x-rays emitted in the presence of an L-shell vacancy decreased with increasing projectile velocity above a projectile-to-L-shell electron velocity ratio of 1 for deuterons and alpha particles. This study was the first to test the applicability of the Gryzinski[59] and BEA[57] models to the description of single K- plus single L-shell ionization. Richard et al.[55] measured the aluminum Kα x-ray yields using 0.4 to 3.0 MeV helium ions. They compared the measured ionization cross sections with the predictions of a modified

BEA model[60] and noted that the gross features of the data were fairly well explained but several areas of disagreement existed. This model assumed that the single K- and multiple L-shell ionization cross section is given by a binomial distribution. Most recently, Hill et al.[52] did a comprehensive study of the projectile atomic number and energy dependence of titanium Kα x-rays and satellites. Beams of 2.5 to 5.0 MeV protons, 4 to 18 MeV helium ions, 10.5 to 26.25 MeV lithium ions, 21 to 45 MeV carbon ions, and 15 to 60 MeV oxygen ions were used to excite thick titanium targets. With the exception of the oxygen ion data, the relative intensities of the satellites produced by the projectiles used in this study showed rough qualitative agreement with the predictions of a theoretical model by Hill and Madison (discussed in Ref. 52). There was poor agreement between the oxygen ion data and the theoretical prediction. This model also assumed a binomial distribution for the multiple ionization cross sections and used empirical correction factors to compensate for underpredictions at small impact parameters.

The objective of this study then is to test the applicability of the SCA and BEA to predict single K- and multiple L-shell ionization over a wide energy range. An extension of the investigation by Richard et al.[55] (0.4 to 3.0 MeV He on aluminum) to much higher energies was made. The aluminum and silicon Kα x-ray spectra resulting from impacts with 5.4 to 40.6 MeV helium ions were measured and the aluminum results compared with the predictions of the BEA and SCA. The Kα x-ray satellite dependence on the energy of heavy ion projectiles was also studied using 21.0 to 74.1 MeV carbon and 23.4 to 117.0 MeV neon ions.

In Chapter II, the projectiles, targets, and experimental procedures used to produce multiple inner-shell vacancies and to detect the x-rays are described. The method of data analysis is presented in Chapter III and the results of this study given in Chapter IV. Finally, three prevailing theories of inner-shell ionization, the plane-wave Born approximation, the semi-classical approximation, and the binary-encounter approximation, will be discussed briefly in Chapter V and the results of the SCA and BEA compared with experimental data. The Appendices contain a computer listing for the Gaussian integration routine used to calculate the theoretical ionization cross sections for the various vacancy configurations and a discussion of the dependence of the sensitivity of x-ray detection on the atomic number and energy of the projectile.

CHAPTER II

EXPERIMENTAL PROCEDURES

A. Beams and Targets

The Texas A&M University variable energy cyclotron was used to accelerate helium ions to energies of 5.4, 6.6, 10.4, 23.2, and 40.6 MeV; carbon ions to energies of 12.0, 22.0, 26.9, 42.9, and 74.1 MeV; and neon ions to energies of 23.4, 41.6, and 117.0 MeV. The beams were extracted from the 88-inch cyclotron and directed down an evacuated beam line to the experimental area by two switching magnets. They were aligned and focused to a spot approximately 0.6 cm in diameter using two sets of quadrupole magnets. Alignment and focusing was observed visually by allowing the beam to strike a fluorescent material (a mixture of zinc sulfide, ZnS, and cadmium sulfide, CdS) placed in the target position and adjusting the current on the quadrupole magnets while monitoring the beam spot with a closed circuit television camera. The camera was located at the side of the target chamber to view the fluorescent target through a plexiglas panel on the target chamber. The camera could be controlled remotely from the cyclotron control room. After the beam had been aligned to the center of the target area and focused, a 0.6 cm diameter collimator was remotely positioned at the front of the target chamber and the fluorescent target replaced by a target of experimental interest. The target assembly consisted of a target wheel capable of holding three targets plus the fluorescent target. The target wheel was remotely controlled and a target was

selected by simply rotating the target wheel until the desired target was in the proper target position. The beam current measured in the target was maintained between 50 and 100 nanoamps.

The aluminum and silicon Kα spectral measurements were performed using thin aluminum and silicon monoxide and thick silicon, silicon monoxide, and silicon dioxide targets. The aluminum targets consisted of self-supporting aluminum foils approximately 2.34 mg/cm^2 thick glued to 2.54 cm diameter aluminum rings. The thin silicon monoxide targets were prepared by vacuum evaporation of silicon monoxide onto thin aluminum backings, and the backings were then glued to 2.54 cm diameter aluminum rings. The thicknesses of these silicon monoxide targets ranged from 0.92 mg/cm^2 to 1.71 mg/cm^2. The thicknesses given above for the aluminum and silicon monoxide targets are the effective thicknesses and have been corrected to account for the 45° inclination of the target with respect to the beam. The thick silicon target was a silicon crystal taken from a retired Si(Li) detector and mounted on a 2.54 cm diameter aluminum ring. The thick silicon monoxide and silicon dioxide targets were prepared by compacting finely ground powders in a pellet press, the resulting pellets (1.3 cm diameter, 0.3 cm thick) were glued to aluminum backings, and the backings were then glued to 2.54 cm diameter aluminum rings.

B. X-ray Measurements

A high resolution plane crystal spectrometer was used in these experiments to obtain the Kα satellite spectra of aluminum and silicon. The spectrometer had been adapted for in-beam use with a high-energy

particle accelerator and was constructed from a design obtained from the Naval Research Laboratory.[61] It is essentially identical to the spectrometer used by Burkhalter et al.[45] and Knudson et al.[25] in previous measurements of ion-induced x-ray spectra.

As shown in Figs. 3 and 4, the crystal spectrometer consists of a flat crystal mounted at the center of a 15.24 cm turntable on which the detector rides. A relationship is maintained between the crystal mount and the turntable such that as the mount rotates through the Bragg angle θ, the turntable rotates through the angle 2θ. A gear train driven by a percision stepping motor maintains the relationship between the crystal mount and the turntable. The detector is thus in the correct position to observe x-rays which satisfy the Bragg relationship

$$n\lambda = 2d \sin \theta, \qquad (2.1)$$

where 2d is double the atomic spacing of the crystal, λ is the wavelength of the x-ray, θ is the angle of reflection from the crystal, and n is the reflection order. Modifications to the spectrometer to allow adjustment of the Bragg crystal and the entrance soller slit alignment remotely can be seen in Fig. 4.

The spectrometer was positioned perpendicular to the incident ion beam, and the target was mounted at 45° with respect to both the ion beam and the spectrometer. The incident x-rays were collimated prior to impinging on the Bragg crystal by a set of commercially available soller slits having a length of 3.18 cm and a plate spacing of 0.127 mm which limited the angular divergence of the x-rays to approximately 0.3°. A similar set of soller slits having a plate spacing of 0.254 mm was used in front of the detector to reduce the background due to

FIG. 3. Crystal spectrometer experimental configuration.

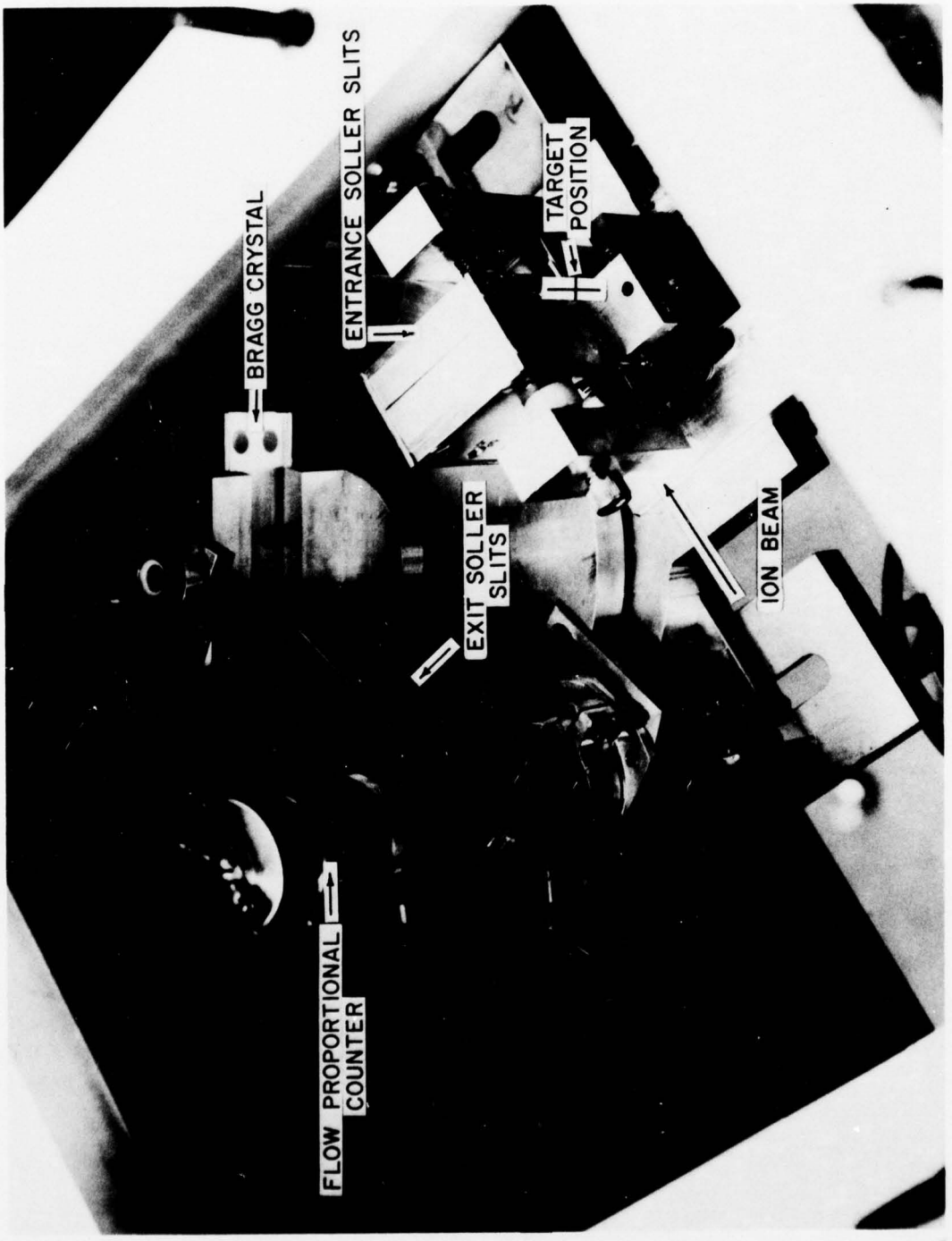
BRAGG CRYSTAL
ENTRANCE SOLLER SLITS
TARGET POSITION
EXIT SOLLER SLITS
ION BEAM
FLOW PROPORTIONAL COUNTER

FIG. 4. Crystal spectrometer with crystal and soller slit adjustments.

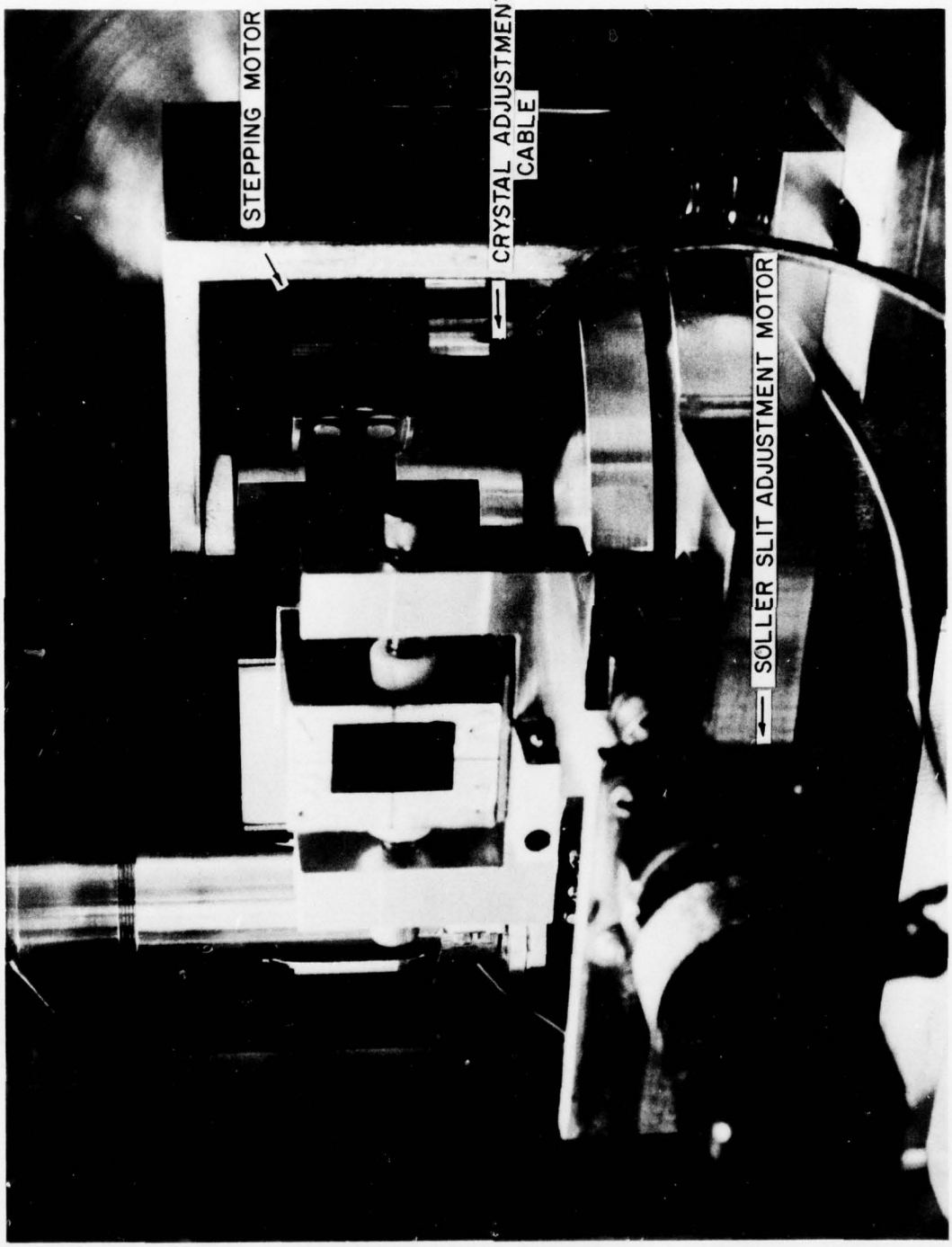
STEPPING MOTOR
CRYSTAL ADJUSTMENT CABLE
SOLLER SLIT ADJUSTMENT MOTOR

scattered x-rays and electrons. Since the best resolution is obtained with a crystal having a 2d spacing only slightly larger than the wavelength of interest, a flat PET (pentaerythritol) crystal was selected for these measurements. The 2d spacing for a PET crystal is 8.75 Å and 7.13 Å respectively. A gas flow proportional counter (90% argon and 10% methane) having an aluminum coated (100 $\mu g/cm^2$) Mylar (530 $\mu g/cm^2$) window was used to detect the reflected x-rays. Lead shielding was placed between the collimators and the spectrometer to reduce the background from particles scattered by the collimators.

Automatic control of the spectrometer was provided by a specially designed system. A schematic diagram of the experimental layout is shown in Fig. 5. Signals from the detector were amplified by a Canberra Model 1417 spectroscopy amplifier and sent to a Canberra Model 1437 timing single channel analyzer where an energy window was set around the x-rays of interest. The output signals from the single channel analyzer were then sent to the spectrometer control where an internal gate permitted passage of the signals to a Northern NS-6300 multichannel pulse height analyzer operated in the external-multiscale mode and to a PDP 15 computer. Passage of the signals was restricted each time the spectrometer rotated to a new counting position and while the multiscalers on the pulse height analyzer and the PDP 15 were being advanced and reset.

A block diagram of the spectrometer control system is shown in Fig. 6. The counting time at each spectrometer angle was determined by a preset number of monitor counts selected on thumbwheel switches located on the front of the spectrometer control. The number of monitor

FIG. 5. Crystal spectrometer experimental layout.

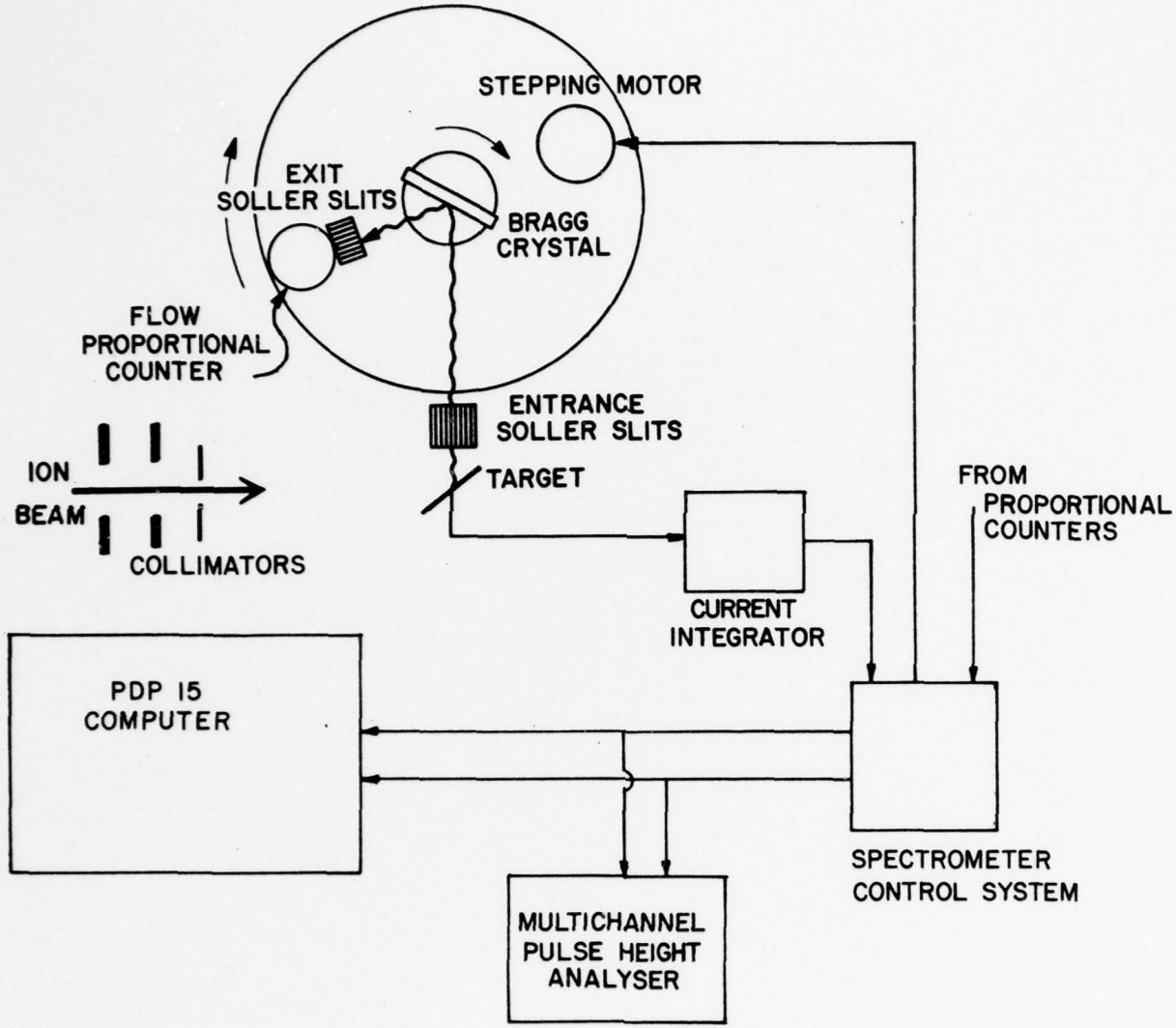
STEPPING MOTOR
EXIT
SOLLER SLITS
BRAGG
CRYSTAL
FLOW
PROPORTIONAL
COUNTER
ENTRANCE
SOLLER SLITS
ION
BEAM
TARGET
COLLIMATORS
FROM
PROPORTIONAL
COUNTERS
CURRENT
INTEGRATOR
PDP 15
COMPUTER
SPECTROMETER
CONTROL SYSTEM
MULTICHANNEL
PULSE HEIGHT
ANALYSER

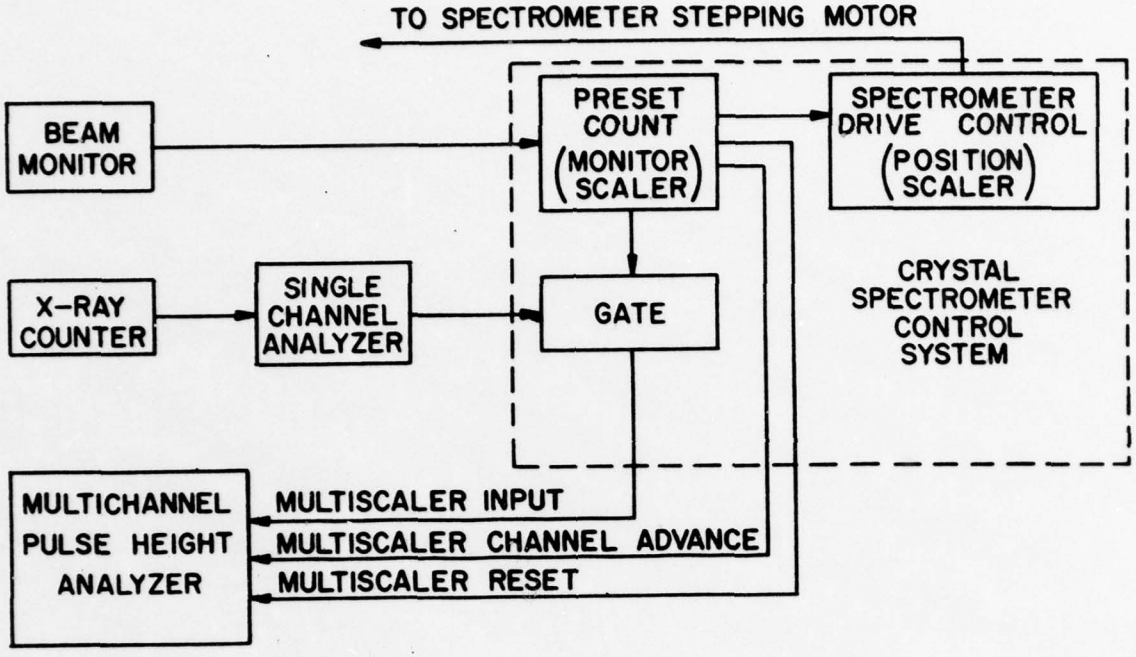

FIG. 6. Block diagram of spectrometer control system.

counts was selected such that approximately 3000 counts above the background were obtained in the peak channel of the satellite of greatest intensity. The monitor counts were generated by a digital current integrator which integrated the current produced in the target by the beam. When the selected number of monitor counts had been collected, the spectrometer control system automatically stepped the spectrometer to the next counting position and advanced and reset the multiscalers on the pulse height analyzer and the PDP 15 computer. The number of steps between one counting position and the next can also be selected by another set of thumbwheel switches on the front panel of the spectrometer control system (9.09×10^{-3} degree/step). Both the number of monitor counts being accumulated and the spectrometer counting position were displayed on the front panel of the spectrometer control system by arrays of light emitting diodes.

The PDP 15 computer provided the capability of on-line data analysis of a previously stored spectrum while a new spectrum was accumulating. The data analysis program was adapted for the PDP 15 during the progress of these experiments and the PDP 15 was used in the later measurements.

CHAPTER III

DATA ANALYSIS

The x-ray signals coming from the spectrometer control system to the pulse height analyzer were recorded in one of 256 channels of the analyzer memory or into one of the storage locations of the PDP 15 computer. Each channel or storage location corresponded to one of the spectrometer counting positions. Prior to the use of the PDP 15, once a spectrum was completed, it was copied onto a magnetic tape by means of a Kennedy Incremental 1600 tape drive unit which was used in conjunction with the pulse height analyzer. The tape was processed on an IBM 7094 computer using a program named DIABOLICAL PLOT which had the capability of reading data tapes from several analyzer systems, producing punched cards containing spectral data, and graphically representing each spectrum by printer plots and/or calcomp plots (linear or semi-log). Using the punched data cards, each spectrum was further analyzed by carrying out a non-linear least-squares fit to the spectrum employing a Gaussian-plus-exponential-tail peak fitting program called AIRLIFT to obtain the relative satellite intensities and peak positions. Further details and discussions of this peak fitting procedure can be found elsewhere.[62-64] An example of the fits typically obtained is shown in Fig. 7. The solid circles represent data points and the open circles represent calculated points.

The first peak, the normal $K\alpha_{1,2}$ peak, was assigned the $K\alpha_{1,2}$ energy given by Bearden.[65] This energy, E_K, is related to the Bragg

FIG. 7. Example of a typically fitted spectrum.

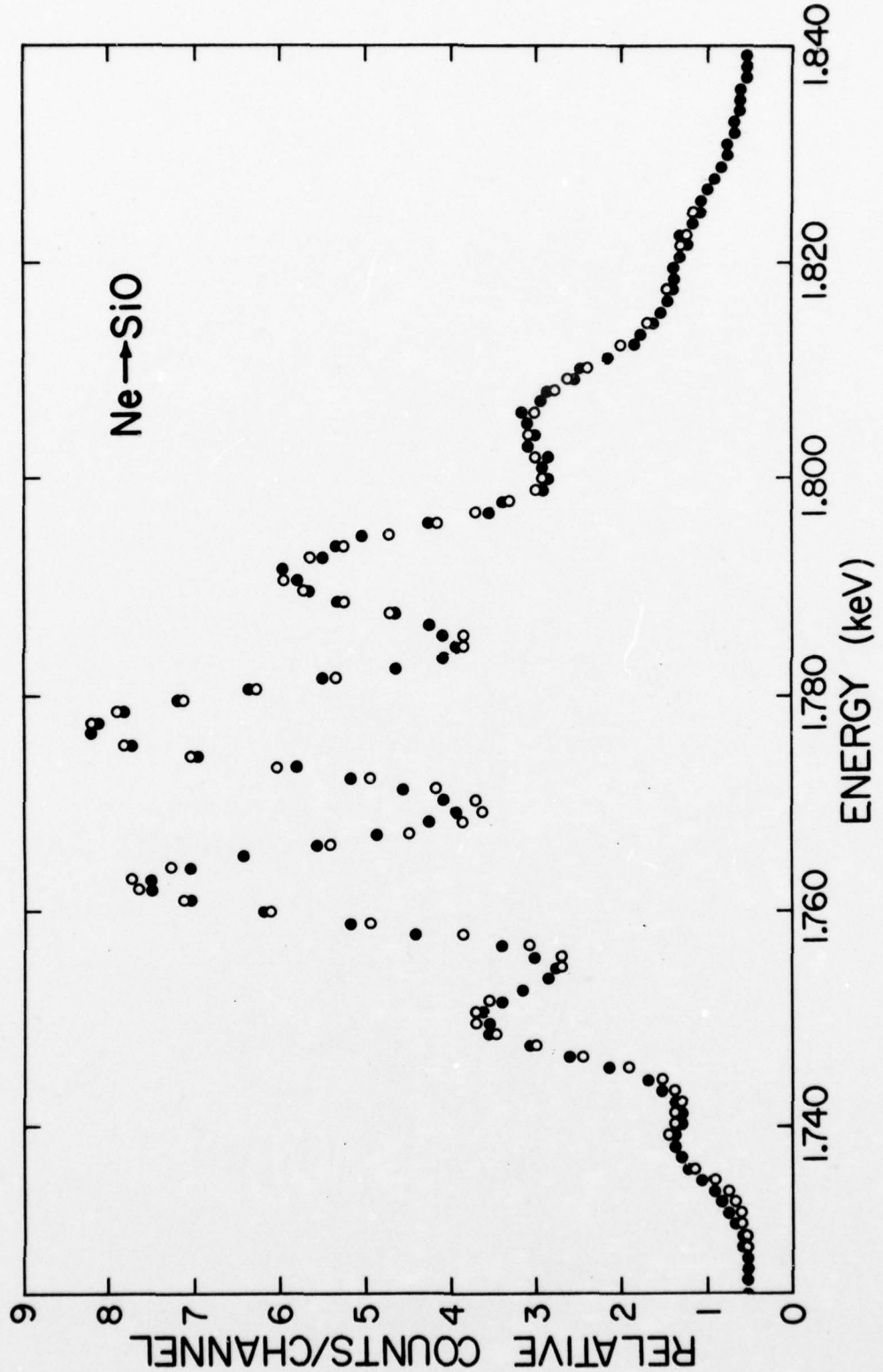
Ne→SiO
RELATIVE COUNTS/CHANNEL
ENERGY (keV)
0
1
2
3
4
5
6
7
8
9
1.740
1.760
1.780
1.800
1.820
1.840

angle, θ_K, by the expression

$$\theta_K = \sin^{-1} \left(\frac{nhc}{2dE_K}\right), \tag{3.1}$$

where n = 1 for first-order reflections and where $\lambda_K = \frac{hc}{E_K}$ has been substituted into Eq. (2.1). In this substitution, λ_K is the wavelength of the Kα x-ray, h is the Planck constant, and c is the speed of light. Any succeeding position on the spectrum corresponds to $\theta_i = \theta_K - \Delta\theta_i$ where $\Delta\theta_i$ can be determined by knowing the number of channels from the $K\alpha_{1,2}$ position, the number of steps per channel selected on the spectrometer control, and the number of degrees per step of the spectrometer. The corresponding energy is then

$$E_i = \frac{nhc}{2d \sin \theta_i} . \tag{3.2}$$

Each peak intensity was corrected for absorption in the target, absorption in the proportional counter window, and for detection efficiency according to the equation

$$I = \frac{N_x}{T_1 T_2 T_3} , \tag{3.3}$$

where I is the corrected peak intensity, N_x is the number of x-rays detected in the photopeak, T_1 is the correction for x-ray absorption in the target, T_2 is the correction for x-ray absorption in the detector window, and T_3 is the detector efficiency for the photopeak. The terms, T_1 and T_2, were determined from the expression

$$T = e^{-ux} , \qquad (3.4)$$

where u is the mass absorption coefficient of the target or the detector window taken from a compilation by Storm and Isreal[66] and x is the effective target or detector window thickness. The detection efficiency was determined by

$$T_3 = 1 - e^{-ux} , \qquad (3.5)$$

where u is the mass absorption coefficient of the detector gas and x is the effective thickness of the detector gas. Since relative intensities and not absolute intensities were measured, corrections for crystal reflectivity efficiency were not made. Also, the crystal reflectivity is not expected to change significantly over the range of angles being scanned for each spectrum (65.4° to 73.2° for aluminum and 46.9° to 50.3° for silicon). The corrections for absorption by the target and detector window and for detection efficiency had a very small effect since only relative intensities were determined and the energy span of each spectrum was less than 120 eV.

The effective thickness for each projectile-target combination was determined by calculating the average depth of x-ray emission from the front of the target. The rate per unit solid angle of x-ray emission from the front of the target is

$$R_t = \frac{R_B f N_A \omega}{W_{at.}} \int_0^t \sigma(x) T(x) dx , \qquad (3.6)$$

where R_B is the incident particle rate, ω is the fluorescence yield, f

is the weight fraction of the element of interest, N_A is Avogadro's number, $W_{at.}$ is the atomic weight of the element of interest, t is the target thickness in g/cm^2, $\sigma(x)$ is the cross section for K-shell ionization at depth x, and $T(x)$ is the transmission correction given by $T(x) = e^{-ux}$. The values of $\sigma(x)$ were calculated by means of the equation

$$\sigma(x) = \sigma_o - \int_0^x \frac{d\sigma}{dE}\frac{dE}{dx}\,dx \ , \tag{3.7}$$

where σ_o is the K-shell ionization cross section for the incident beam energy. The average depth of x-ray emission through the front of the target is then given by

$$\bar{x} = \frac{\int_0^x x\sigma(x)T(x)dx}{\int_0^x \sigma(x)T(x)dx} \ . \tag{3.8}$$

The binary encounter model results of Garcia[67] were used to obtain σ_o and $d\sigma/dE$, and the dE/dx values were derived from the stopping-power tables of Northcliffe and Schilling.[68] Also, it was necessary to determine the average projectile energy for x-ray emission. The average projectile energy for the emission of K x-rays through the front of the target was calculated from the relationship

$$\bar{E} = \frac{\int_0^t E(x)T(x)\sigma(x)dx}{\int_0^t T(x)\sigma(x)dx} \ , \tag{3.9}$$

$$\text{where } E(x) = E_o - \int_0^x \frac{dE}{dx}\,dx \ . \tag{3.10}$$

In Eq. (3.10), E_o is the incident beam energy. The effective target thicknesses and the average projectile energies were calculated using a computer program, ORION.[69]

For the purpose of making detailed comparisons of the Kα x-ray satellite intensity distributions in this study, it is convenient to use a parameter which shall be referred to as the apparent average L-vacancy fraction, p_L.[70] This parameter, p_L, is defined as

$$p_L \equiv \frac{\bar{n}}{N_L} = \frac{1}{N_L} \Sigma\, n f_n \,, \qquad (3.11)$$

where n is the number of L-shell vacancies, N_L is the number of L-shell electrons in the ground-state atom, and f_n is the fraction of the total Kα x-ray yield contained in the nth satellite peak. The value, p_L, does not directly represent the average fraction of L-shell vacancies at the time of Kα x-ray emission since the fluorescence yields differ for the various vacancy configurations. However, this parameter has been chosen since it has been shown[38,40] that the intensity pattern of the Kα satellite lines can be well represented by binomial distributions in which the relative intensity of each satellite peak is approximately given by the formula

$$f_n = \frac{I_n}{I_{tot}} \simeq \binom{N_L}{n} p_L^n (1 - p_L)^{N_L - n} \,, \qquad (3.12)$$

where $\binom{N_L}{n} = \frac{N_L!}{(N_L - n)!n!}$, I_n is the number of x-rays detected in the nth satellite peak, and I_{tot} is the total number of x-rays detected.

CHAPTER IV

RESULTS

Kα x-ray spectra obtained in the present work illustrating the dependence of the p_L values on the projectile atomic number are shown in Figs. 8 and 9. As the atomic number of the projectile is increased, the intensity distribution shifts to the higher order satellites yielding higher p_L values. This effect has been noted previously using thick[40,71] and thin[51] targets. In the neon on silicon monoxide spectrum in Fig. 8, seven peaks are discernible whereas in the aluminum spectra in Fig. 9 using carbon, oxygen, and neon ions, only six are discernible. The rapid attenuation of the sixth and seventh satellite peaks in the aluminum spectra is attributed to the K absorption edge occuring at 1559.6 eV.

The dependence of p_L on the velocity of the projectile is shown in Figs. 10 and 11. Fig. 10 illustrates the velocity dependence with light (helium) ions and Fig. 11 with heavier (oxygen) ions. In both situations, as the projectile energy is increased, the intensity distribution shifts to the lower order satellites or to a lesser degree of L-shell ionization. A study by Li *et al.*[49] showed that for deuterons and helium ions on calcium, the fraction of Kβ x-rays emitted in the presence of L-shell vacancies reached a maximum at a projectile-to-L-shell electron velocity ratio of about 1. The results of Richard *et al.*[55] studying the Kα x-rays from helium ions on aluminum showed that maximum L-shell ionization in the presence of a single K-shell vacancy

FIG. 8. Silicon Kα x-ray spectra produced by He, C, O, and Ne ions.

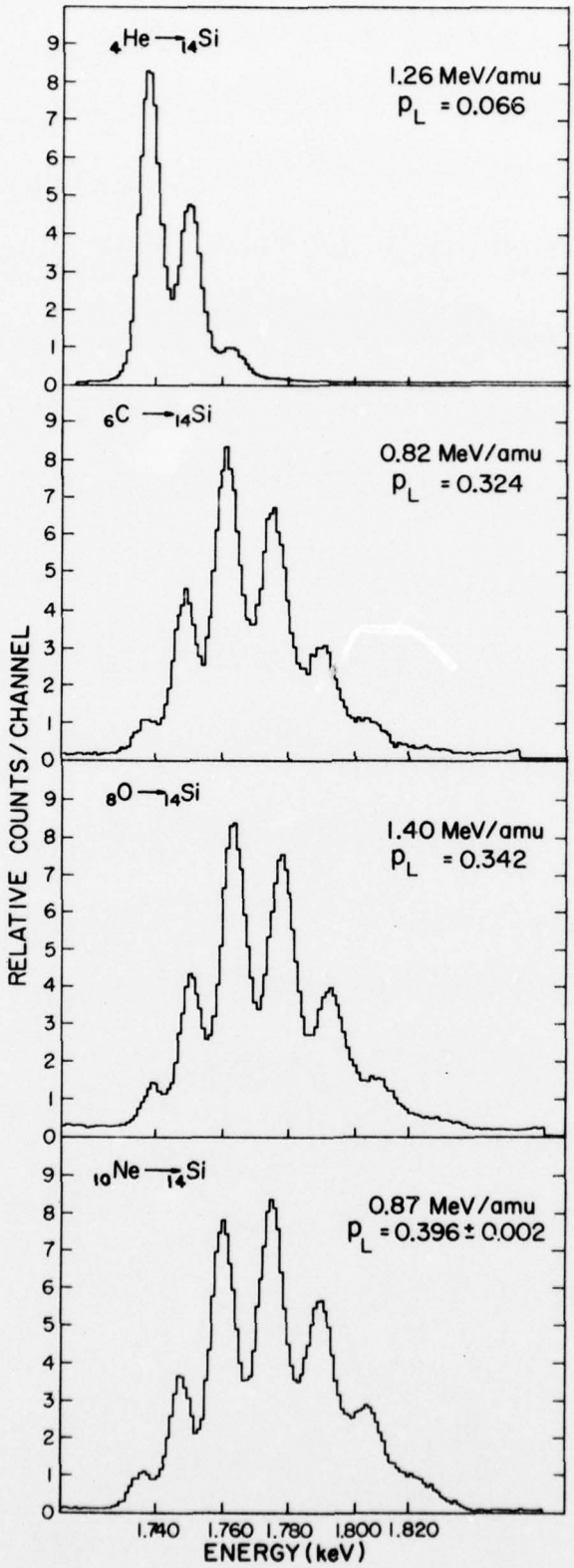
$_4$He → $_{14}$Si
1.26 MeV/amu
p_L = 0.066
$_6$C → $_{14}$Si
0.82 MeV/amu
p_L = 0.324
$_8$O → $_{14}$Si
1.40 MeV/amu
p_L = 0.342
$_{10}$Ne → $_{14}$Si
0.87 MeV/amu
p_L = 0.396 ± 0.002
RELATIVE COUNTS/CHANNEL
1.740 1.760 1.780 1.800 1.820
ENERGY (keV)

FIG. 9. Aluminum Kα x-ray spectra produced by He, C, O, and Ne ions.

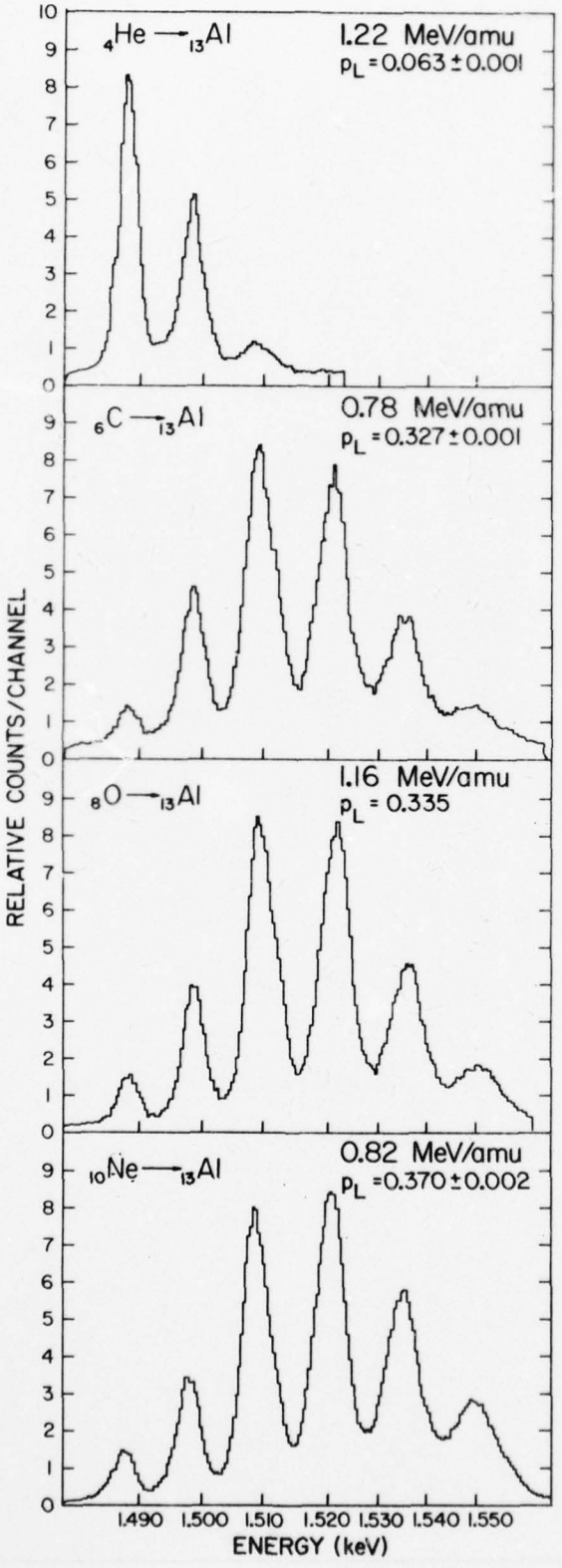
$_4$He → $_{13}$Al
1.22 MeV/amu
p_L = 0.063 ± 0.001
$_6$C → $_{13}$Al
0.78 MeV/amu
p_L = 0.327 ± 0.001
$_8$O → $_{13}$Al
1.16 MeV/amu
p_L = 0.335
$_{10}$Ne → $_{13}$Al
0.82 MeV/amu
p_L = 0.370 ± 0.002
RELATIVE COUNTS/CHANNEL
1.490 1.500 1.510 1.520 1.530 1.540 1.550
ENERGY (keV)

FIG. 10. Kα x-ray satellite dependence on the projectile energy produced by light (He) ions.

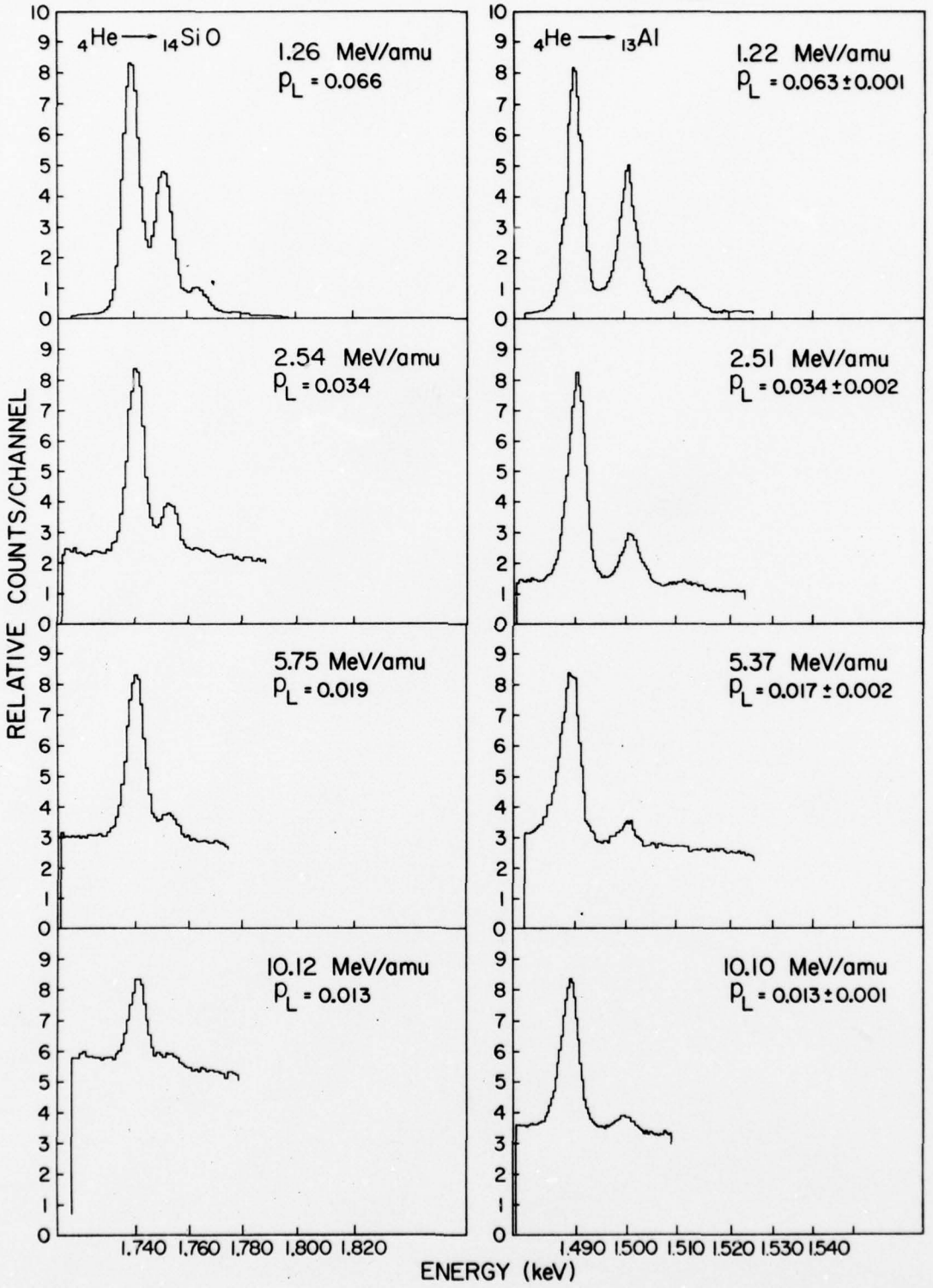
$^4He \rightarrow {}_{14}Si\,O$
1.26 MeV/amu
$P_L = 0.066$
2.54 MeV/amu
$P_L = 0.034$
5.75 MeV/amu
$P_L = 0.019$
10.12 MeV/amu
$P_L = 0.013$
$^4He \rightarrow {}_{13}Al$
1.22 MeV/amu
$P_L = 0.063 \pm 0.001$
2.51 MeV/amu
$P_L = 0.034 \pm 0.002$
5.37 MeV/amu
$P_L = 0.017 \pm 0.002$
10.10 MeV/amu
$P_L = 0.013 \pm 0.001$
RELATIVE COUNTS/CHANNEL
1.740 1.760 1.780 1.800 1.820
1.490 1.500 1.510 1.520 1.530 1.540
ENERGY (keV)

FIG. 11. Kα x-ray satellite dependence on the projectile energy produced by heavy (O) ions.

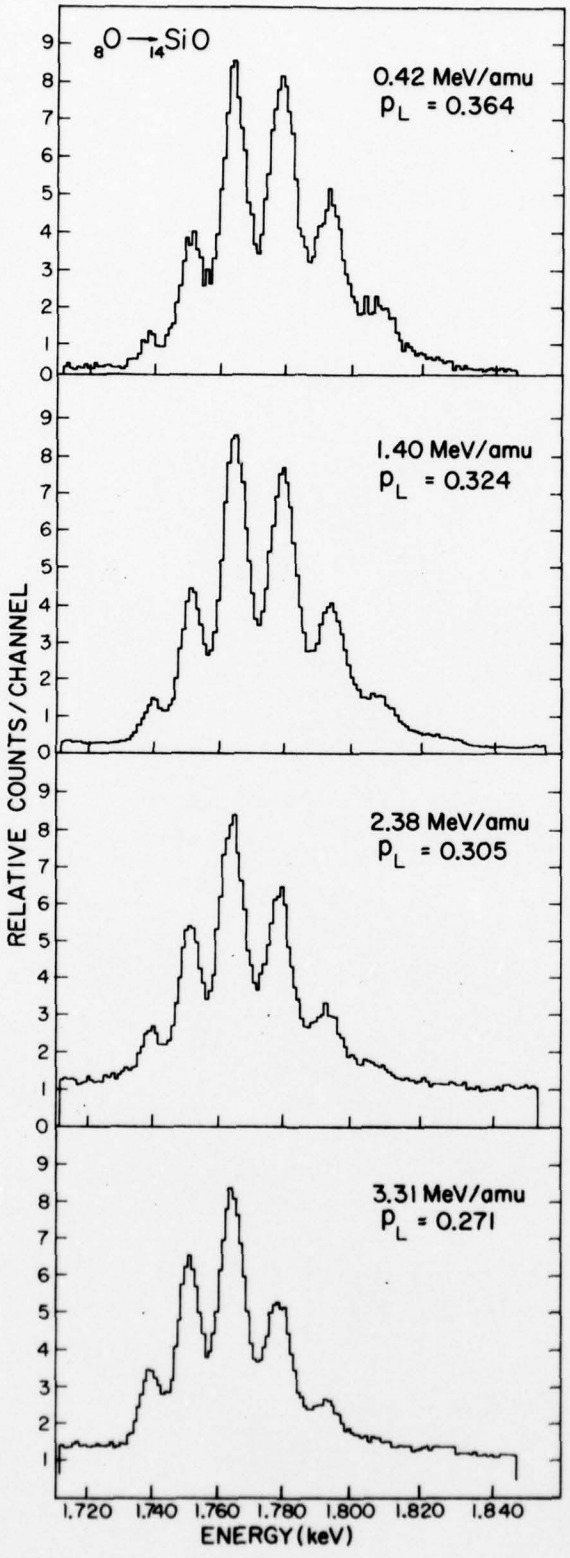
$_8O \rightarrow _{14}SiO$
0.42 MeV/amu
p_L = 0.364
1.40 MeV/amu
p_L = 0.324
2.38 MeV/amu
p_L = 0.305
3.31 MeV/amu
p_L = 0.271
RELATIVE COUNTS/CHANNEL
1.720 1.740 1.760 1.780 1.800 1.820 1.840
ENERGY (keV)

occured at a velocity ratio of approximately 1.25. The investigation by Knudson et al.[54] of Kα x-rays from low energy neon ions on aluminum indicated that maximum L-shell ionization in the presence of one K-shell vacancy occurs above a velocity ratio of 2. From these results, it is evident that the velocity ratio for maximum L-shell ionization in the presence of a K-shell vacancy is dependent upon the atomic number of the projectile. In this study, ions having energies above the velocity ratio for maximum L-shell ionization were used and thus, in Fig. 10, the p_L values decrease with increasing projectile energy. This is qualitatively the behavior expected on the basis of the velocity dependence of the cross section for L-shell ionization.

In Figs. 10 and 11, the dependence of the peak to background ratio on the projectile energy may also be observed. The background rapidly increases as the projectile energy increases. In Fig. 10, a higher rate of increase of the background in the silicon monoxide spectra than in the aluminum spectra is seen. The more rapid rate of increase is a result of the lower Coulomb barrier for helium ions on the oxygen atoms in the silicon monoxide target compared with the Coulomb barrier of helium ions on aluminum atoms. Nuclear reactions can occur at lower energies in the silicon monoxide target and thus, the more rapid rate of increase of the background with increasing projectile energy. (A further discussion of peak to background measurements can be found in Appendix B.)

The measured Kα x-ray relative intensities are listed in Table I for helium, carbon, and neon ions on aluminum and silicon. Also listed in this table are the incident projectile energies, the average

TABLE I. Relative Kα x-ray intensities and p_L values.

Projectile and Compound	f_n n=0	n=1	n=2	n=3	n=4	n=5	n=6	NOM	$\bar{E}$	p_L
5.42 MeV He										
Al	0.580	0.336	0.084					5	4.86	0.063±0.001
SiO	0.550	0.371	0.079					6	5.04	0.066±0.001
6.64 MeV He										
Al	0.643	0.285	0.064					3	6.14	0.052±0.002
SiO	0.630	0.317	0.053					3	6.61	0.053±0.001
10.40 MeV He										
Al	0.761	0.208	0.032					3	10.03	0.034±0.002
SiO	0.753	0.219	0.029					3	10.05	0.035±0.003
23.20 MeV He										
Al	0.865	0.135						5	22.94	0.017±0.0005
SiO	0.849	0.151						5	23.03	0.019±0.0007
40.60 MeV He										
Al	0.895	0.105						5	40.45	0.013±0.0005
SiO	0.896	0.104						5	40.48	0.013±0.001
12.00 MeV C										
Al	0.029	0.120	0.337	0.292	0.161	0.061		3	9.35	0.327±0.002
SiO	0.027	0.151	0.308	0.304	0.138	0.073		3	9.81	0.324±0.0002
22.00 MeV C										
Al	0.058	0.181	0.377	0.251	0.105	0.029		3	18.51	0.282±0.001
SiO	0.061	0.238	0.377	0.235	0.087			3	18.77	0.256±0.003
26.90 MeV C										
Al	0.078	0.219	0.396	0.223	0.084			3	23.58	0.252±0.001
SiO	0.076	0.274	0.352	0.277	0.071			3	24.83	0.243±0.001
42.9 MeV C										
Al	0.177	0.318	0.344	0.129	0.033			4	40.31	0.190±0.002
SiO	0.172	0.373	0.304	0.127	0.024			7	41.23	0.182±0.001
74.1 MeV C										
Al	0.316	0.360	0.324					4	72.27	0.126±0.003
SiO	0.350	0.438	0.213					4	72.88	0.108±0.0006
23.4 MeV Ne										
Al	0.032	0.081	0.254	0.289	0.220	0.124		5	17.81	0.370±0.002
SiO	0.021	0.092	0.221	0.281	0.189	0.143	0.053	3	19.80	0.395±0.001
46.1 MeV Ne										
Al	0.055	0.089	0.278	0.279	0.196	0.103		3	34.05	0.348±0.0007
SiO	0.040	0.106	0.247	0.286	0.172	0.112	0.037	3	36.56	0.366±0.0002
117.0 MeV Ne										
Al	0.142	0.226	0.332	0.216	0.070	0.011		3	112.62	0.235±0.002
SiO	0.121	0.253	0.330	0.211	0.069	0.017		3	114.11	0.238±0.001
22.00 MeV C										
Si(Thick)	0.057	0.225	0.347	0.270	0.102			3	17.29	0.267±0.001
SiO(Thick)	0.058	0.230	0.357	0.260	0.095			3	17.81	0.263±0.001
SiO_2(Thick)	0.062	0.234	0.366	0.253	0.084			3	18.04	0.258±0.001

projectile energy for x-ray emission and detection ($\bar{E}$), the number of measurements taken for each compound or element at the given projectile energy (NOM), and the p_L values. The f_n values (the ratio of the nth satellite peak intensity to the sum of the intensities of all the Kα peaks) have been corrected for absorption in the target and detector window, and for detection efficiency. The p_L values were determined directly from the f_n values and the indicated errors are standard deviations. Table I shows numerically the shift in the intensity distribution to the lower order satellites with increasing projectile energy.

Also listed in Table I are the relative intensities and p_L values for 22.0 MeV (incident energy) carbon ions on thick silicon, silicon monoxide, and silicon dioxide targets. The variations of the intensity distributions and the p_L values from one target to the next indicate differing average L-shell vacancies at the time of Kα x-ray emission. The differing average L-shell vacancies at the time of Kα x-ray emission may be associated with the vacancy production process which occurs during collision, or with the deexcitation process. Earlier investigations[39,47] have indicated that at the beam energies used in these measurements, it is quite improbable that the chemical environment of the target atom could influence the vacancy distribution produced during the collisions. The studies have also indicated that these variations may be attributed to intra- and interatomic transitions occuring prior to Kα x-ray emission. These transitions can contribute in a major way to K- and L-shell vacancy filling in multiply ionized atoms.

A plot of the p_L values as a function of the velocity ratio for the

target-projectile combinations listed in Table I is shown in Fig. 12. The velocity ratio was calculated from the expression

$$\frac{V_1}{\bar{V}_L} = \left(\frac{m_o}{M} \frac{\bar{E}_1}{\bar{U}_L} \right)^{\frac{1}{2}} , \qquad (4.1)$$

where V_1 is the average projectile velocity for x-ray emission with energy $\bar{E}_1$, $\bar{V}_L$ is the weighted average of the velocities of the L-shell electrons, m_o is the electron rest mass, M is the mass of the projectile, and $\bar{U}_L$ is the weighted average of the L-shell electron binding energies. The L-shell binding energies used in this calculation were taken from a tabulation by Bearden and Burr.[72]

The dependence of p_L on the energy and atomic number of the projectile and on the atomic number of the target atom is shown in Fig. 12. As the projectile energy increases, the p_L values decrease. As the projectile atomic number increases, the p_L values increase. Finally, as the atomic number of the target increases, the p_L values decrease. Also shown in Fig. 12 is the flattening of the curves with increasing projectile atomic number and the apparent convergence of the heavy ion data at low energies as the region of maximum p_L is approached. This is suggestive of a saturation effect in which the x-ray spectra and subsequent p_L values reach a point where they no longer reflect the initial vacancy distribution as a result of L-shell vacancy filling.

The p_L values for helium ions on aluminum corrected for fluorescence yield are shown in Fig. 13. The low energy data, indicated by open circles, and the fluorescence yields were obtained from a previous study

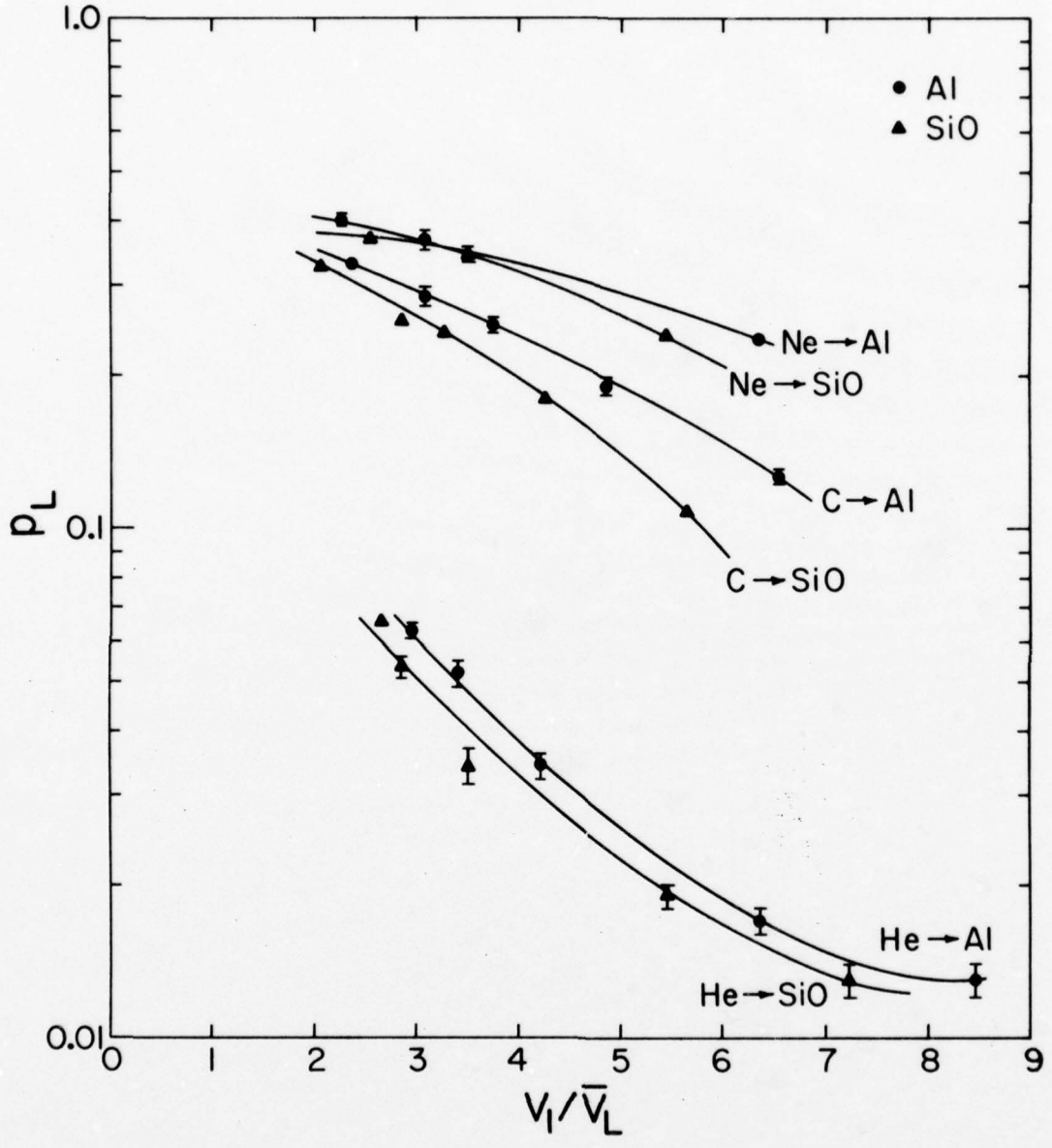

FIG. 12. Variation of p_L with projectile energy for Al and SiO targets.

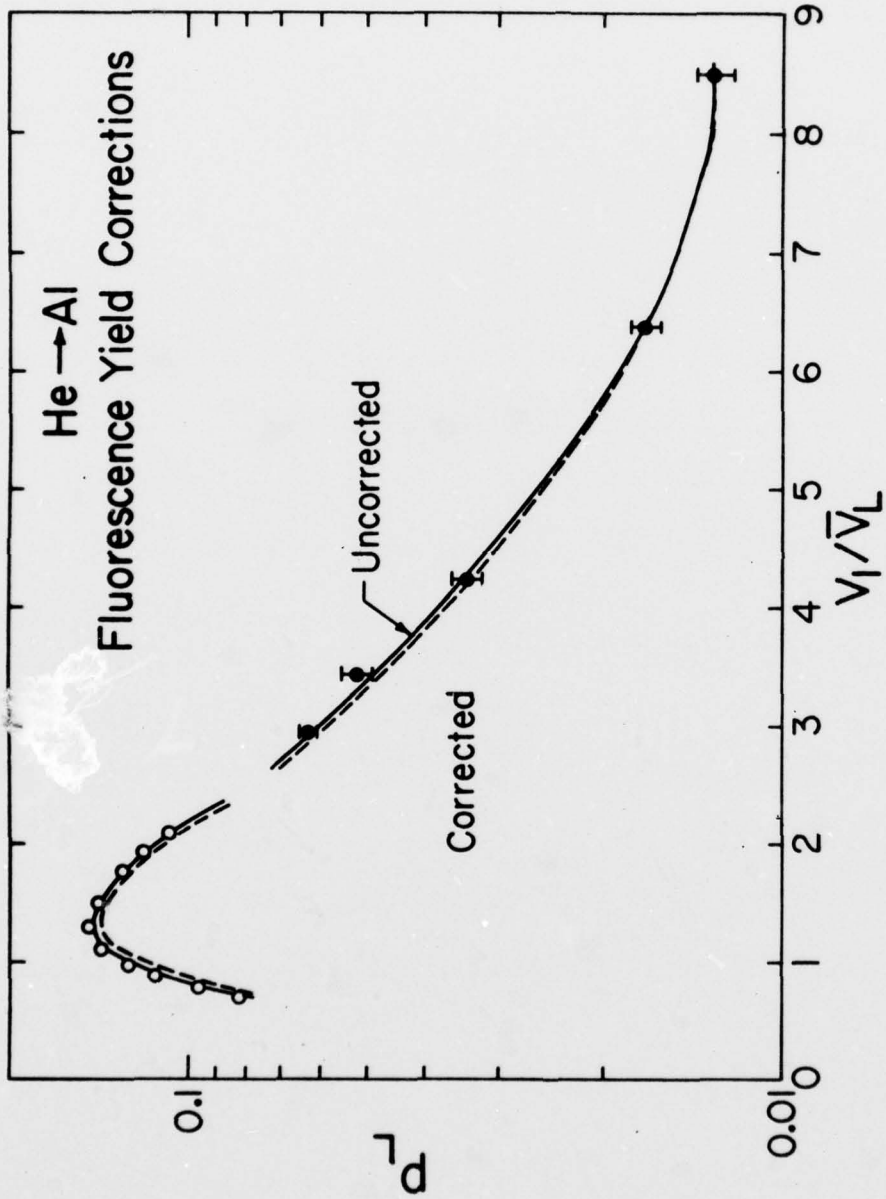

FIG. 13. The P_L values for He ions on Al corrected for fluorescence yield.

by Richard et al.[55] The fluorescence corrections were made according to the expression

$$I'_n = \frac{I_n}{\omega_{KL^n}}, \qquad (4.2)$$

where I_n is the intensity of the nth satellite, I'_n is the corrected intensity of the nth satellite, and ω_{KL^n} is the fluorescence yield for the vacancy configuration with one K-shell and n L-shell vacancies. The fluorescence yields used for the various configurations were 0.041, 0.042, and 0.044 corresponding to n=0, 1, and 2 respectively.[55] An assumption made by Richard et al.[55] in the determination of the fluorescence yield was that the L-shell vacancies were in the L_{II} and L_{III} subshells (2p electrons). This assumption is not entirely valid and some errors will be introduced into the fluorescence yield corrections. It is apparent that the fluorescence yield corrections do not change the features of the curve in a significant way for the low states of ionization involved for this projectile-target combination (an average of 1.2 L-shell vacancies in the atoms of the highest state of ionization shown in Fig. 13).

CHAPTER V

COMPARISON WITH THEORY

A. General Formulations

The collision of an energetic projectile ion with a stationary target atom generally results in the transfer of some of the energy of the projectile to the target atom. Frequently, this energy transfer results in the ionization of one or more inner-shell electrons. Most simple models of inner-shell ionization begin with the assumption that the production of an inner-shell vacancy occurs as a result of the direct Coulomb interaction of the incident particle with the bound electron. Three such models - the plane wave Born approximation (PWBA),[73,74] the impulse or binary-encounter approximation (BEA),[57,67,75-77] and the semi-classical approximation (SCA)[78] - will be briefly discussed here and the results of two, the BEA and SCA, will be compared with experimental data.

The PWBA and BEA are high energy formulations and are expected to be valid for incident particles with energies much greater than the binding energy of the atomic electron. The high energy criterion for these approximations is generally given as[74,79]

$$\frac{z_1 z_2 e^2}{\hbar v_1} \ll 1 , \qquad (5.1)$$

where z_1 is the atomic number of the projectile, z_2 is the atomic number of the target, e is the charge of the electron, $\hbar$ is the Planck constant divided by 2π, and v_1 is the projectile velocity.

The first order plane wave Born approximation assumes that; 1) the projectile acts as a point charge (the effect of the atomic structure of the projectile on vacancy production is negligible), 2) plane waves can be used to describe the incident and scattered particle over all space, and 3) the electron transition is from the bound state to the continuum with the other electrons remaining in their initial states. The ionization cross sections for helium on aluminum predicted by the PWBA can be calculated by[74]

$$\sigma_i = \frac{8\pi n_i z_1^2 a_o^2}{z_{eff}^4 \eta_i} f_i(\theta_i, \eta_i) , \qquad (5.2)$$

where n_i is the number of electrons in the i-th shell, z_1 is the projectile atomic number, a_o is the Bohr radius, z_{eff} is the charge of the target nucleus corrected for screening by the inner-shell electrons, and f_i are form factors calculated using non-relativistic hydrogenic wave functions. These form factors have heen calculated and tabulated as functions of θ_i and η_i by Khandelwal *et al.*[80] and Choi *et al.*[81] for the K- and L-shells, and were used to determine the PWBA ionization cross sections shown in Figs. 14 and 15. The quantity, θ_i, the ratio of the true binding energy of the electron to that predicted by a screened hydrogenic wave function, is determined by the expression

$$\theta_i = \frac{i^2 u_i}{z_{eff}^2 R_\infty} , \qquad (5.3)$$

where i is the principle quantum number of the shell, u_i is the binding energy of the i-th electron, and R_∞ is the Rydberg constant. The

FIG. 14. Theoretical K-shell ionization cross sections.

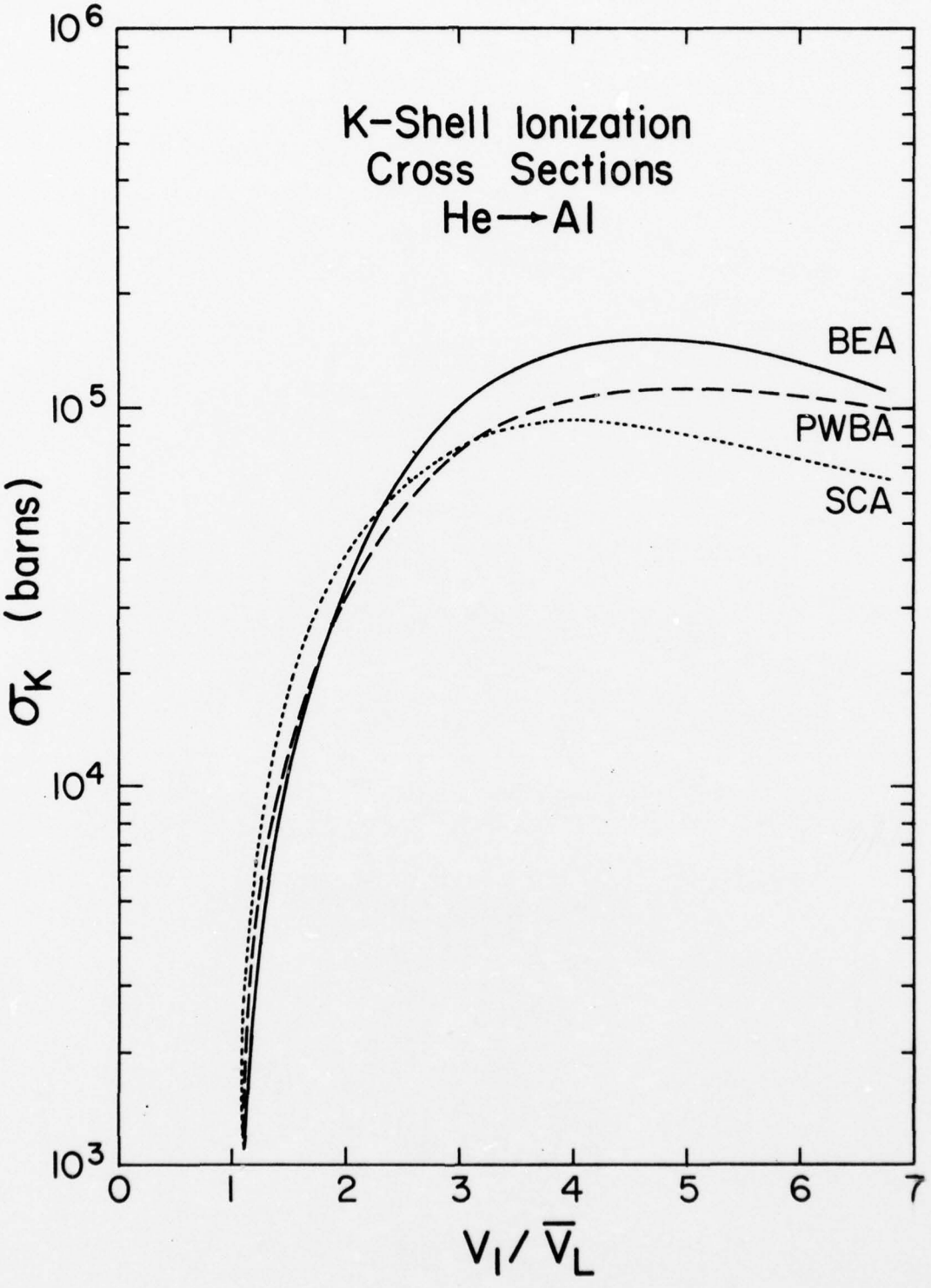
K-Shell Ionization
Cross Sections
He → Al
BEA
PWBA
SCA
10^6
10^5
10^4
10^3
σ_K (barns)
0
1
2
3
4
5
6
7
$V_1 / \overline{V}_L$

FIG. 15. Theoretical L-shell ionization cross sections.

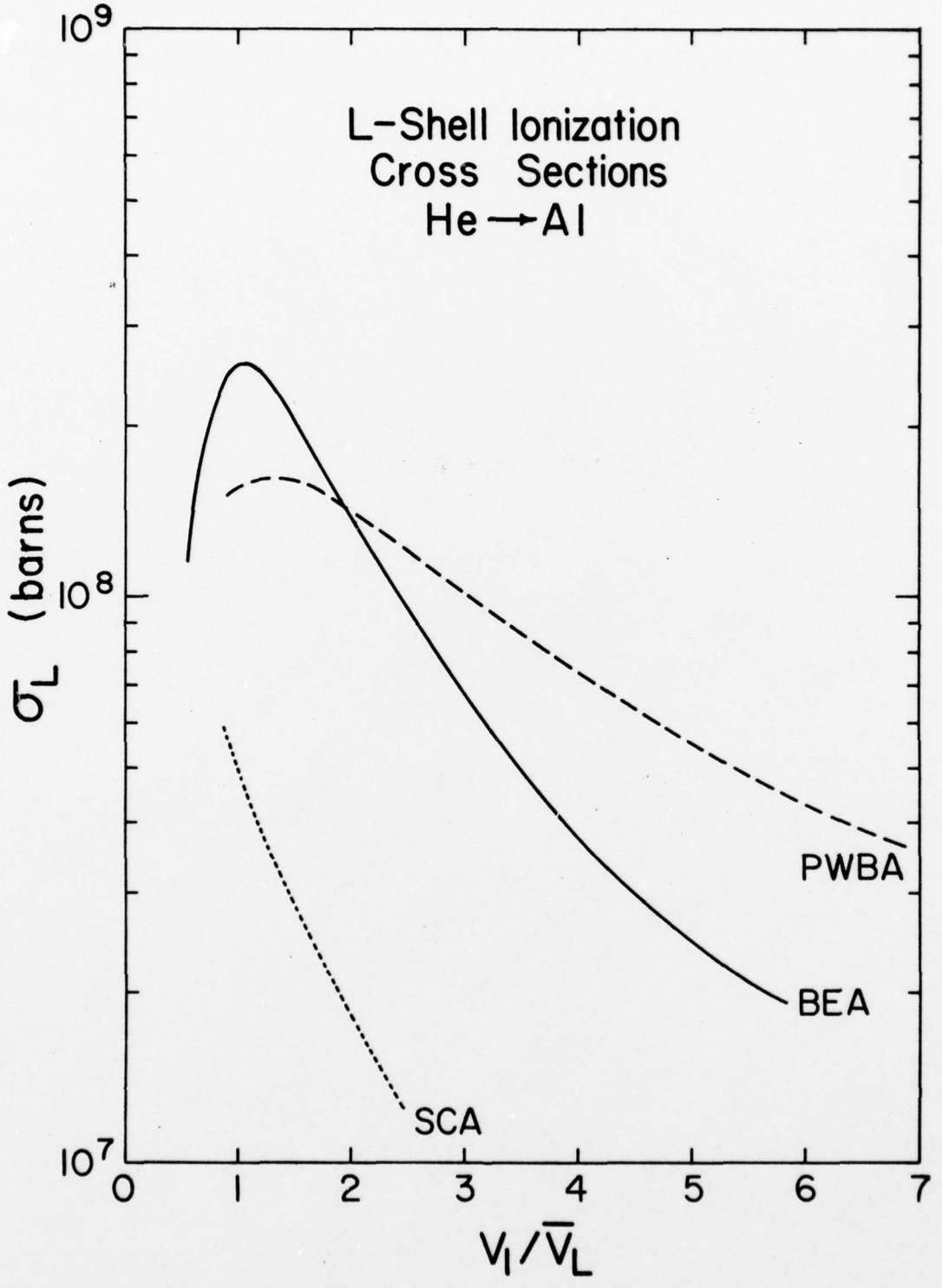
L-Shell Ionization
Cross Sections
He → Al
10^9
10^8
10^7
σ_L (barns)
PWBA
BEA
SCA
0
1
2
3
4
5
6
7
$V_1/\bar{V}_L$

quantity, η_i, is given by the expression

$$\eta_i = \frac{1}{z_{eff}}\left(\frac{h\nu_1}{e^2}\right) = \frac{m_o}{M_1}\frac{E_1}{z_{eff}^2 R_\infty} , \qquad (5.4)$$

where m_o is the rest mass of the electron and M_1 and E_1 are the mass and energy of the projectile respectively.

In the impulse or binary-encounter approximation, ionization is treated classically as a collision between the projectile and a free electron. The result of the collision is a direct energy transfer or exchange between the charged particle and the electron. All other interactions are neglected and the target nucleus exists simply to establish a momentum distribution for the electron. Thomas[82] and Garcia[83] have adjusted this model to take into account the effects of nuclear repulsion between the projectile and the target nucleus. Garcia *et al.*[67,83] have shown that if hydrogenic velocity distributions are used for the exchange of energy between the two particles, the BEA ionization cross sections for the i-th shell obeys a scaling law

$$u_i^2 = z_1^2 f\left(\frac{E_1}{u_i}\right) , \quad \text{for } \frac{m}{M} << 1. \qquad (5.5)$$

Thus, the product of the binding energy squared times the ionization cross section divided by z_1^2 is a universal function of the incident projectile energy expressed in units of the binding energy. Using a semi-relativistic velocity ratio,

$$\frac{v_1}{v_L} = \frac{E_1}{M}\left[\frac{1}{1 - \left(\frac{m_o c}{u_i + m_o c}\right)c^2}\right] , \qquad (5.6)$$

in place of the classical velocity ratio, and performing a linear interpolation in Garcia's tables,[83] the BEA cross sections for helium ions on aluminum were determined for the K-shell (Fig. 14). The BEA L-shell ionization cross sections for helium ions on aluminum were obtained from a tabulation of similar calculations by Hansen[57] and are shown in Fig. 15.

The impact parameter or semi-classical approximation was formulated by Bang and Hansteen[78] to treat ion-atom collisions that did not satisfy the high energy criterion of Eq. (5.1). This treatment is identical to the PWBA with the exception that corrections are made for the deflection of the projectile near the target nucleus as a result of Coulomb repulsion. The repulsion prevents the projectile from penetrating too closely to the target nucleus and thus, cross sections lower than the PWBA predictions can be expected. The SCA predictions of the K- and L-shell ionization cross sections for helium ions on aluminum are given in Figs. 14 and 15 and were determined by[84]

$$\sigma_i = g \frac{z_1^2}{z_{eff}^4 \theta_i} F_i \ , \qquad (5.7)$$

where g is equal to unity for the K-shell and L_I-subshell, 2/3 for the L_{II}-subshell, and 4/3 for the L_{III}-subshell, and z_{eff} is the screened nuclear charge given by

$$z_{eff} = z_2 - S \ , \qquad (5.8)$$

where S is the Slater screening coefficient for the shell being ionized. The term, θ_i, is identical to Eq. (5.3). The values of F_i were obtained from a tabulation by Kocbach[84] as a function of x where x is determined

by

$$x = \frac{z_2 \theta_i}{i(\frac{E_1}{M})} \quad . \tag{5.9}$$

The shapes and magnitudes of the PWBA, BEA, and SCA predictions for K-shell ionization cross sections shown in Fig. 14 are comparable. An unexpected feature in Fig. 14 is the difference between the PWBA and SCA curves. One would expect the SCA predictions to be lower than the PWBA predictions at lower energies, and comparable at higher energies. In Fig. 14, the SCA predictions are slightly higher at lower energies and considerably lower at the higher energies.

The PWBA, BEA, and SCA differ greatly in predicting the shape and magnitude of the dependence of L-shell ionization on the velocity ratio. In Fig. 15, the PWBA and BEA predictions of the shape of the dependence of the ionization cross section on the velocity ratio differ considerably, however, the overall trend of the curves are similar. The SCA predictions, on the other hand, are as much as an order of magnitude lower than the PWBA and BEA predictions and show no indication of a maximum at the lowest velocities for which tabulated values of F_i are avaibable.

B. BEA L-Shell Ionization Probabilities

The BEA probability for ionization of an L-shell electron as a function of impact parameter was obtained using a computer program, BEACON, by Hansen.[57] In the Hansen impact parameter representation of the BEA, the ionization cross section of the i-th shell, σ_i, is related

to the total ionization probability, P_i, by

$$\sigma_i = \int_0^\infty 2\, P_i(b)db \ . \qquad (5.10)$$

The probability of ionization per electron, p_i, is related to the total probability by

$$P_i(b) = 1 - [1-p_i(b)]^n \ , \qquad (5.11)$$

where n is the number of electrons in the i-th shell.

At selected energies, the probabilities of ionization per electron for helium ions on aluminum were obtained as a function of impact parameter for the K- and L-shells (2s and 2p electrons). The L-shell probabilities were summed at given impact parameters and divided by the number of L-shell electrons to obtain the average probability per electron as a function of impact parameter.

C. SCA L-Shell Ionization Probabilities

The SCA probability for ionization of an L-shell electron as a function of impact parameter for a given shell or subshell, i, and characterized by the hydrogenic quantum numbers, n_i, ℓ_i, were determined by

$$P(b) = \mu_{n_i,\ell_i}(\theta_i,\chi_i)\frac{2j_i+1}{2\ell_i+1}\frac{1}{z_i^2\theta_i} I_{n_i,\ell_i}(\chi_i,\beta_i) \ , \qquad (5.12)$$

where j_i is the angular momentum of the shell or subshell, θ_i is described in Eq. (5.3), and z_i is described in Eq. (5.8). The values of χ_i were calculated by

$$\chi_i = \frac{z_i \theta_i}{n_i E_1^{1/2}} , \qquad (5.13)$$

where n_i here is the principle quantum number of shell, i, and E_1 is the projectile energy in MeV. The values of β_i were determined by the expression

$$\beta_i = \frac{bz_i}{n_i a_o} . \qquad (5.14)$$

The values for $\mu_{n_i,\ell_i}(\theta_i,\chi_i)$ and $I_{n_i,\ell_i}(\chi_i,\beta_i)$ were then obtained from a tabulation by Hansteen et al.[58] as functions of θ_i and χ_i, and χ_i and β_i respectively and substituted into Eq. (5.12) to obtain the ionization probabilities as a function of impact parameter. Using this procedure, the ionization probabilities for protons on aluminum were determined. Simple z^2 scaling was used to predict the ionization probabilities for helium ions on aluminum. At each energy, the probabilities as a function of impact parameter were obtained for the K-shell and the L_I-, L_{II}-, and L_{III}-subshells. The L-subshell probabilities were summed at the given impact parameter and divided by the number of L-shell electrons to obtain the average probability per electron as a function of impact parameter.

D. Comparison of Theoretical Predictions with Experimental Data

Polynomial fits using a computer program, POLLY, were made to the calculated points of the probabilities of ionization per electron as a function of impact parameter for each shell (K- and L-shells) to obtain

the functions, $P_K(b)$ and $\bar{P}_L(b)$. The functions $P_K(b)$ and $\bar{P}_L(b)$ are then the probability per electron of ionizing one K-shell electron and the average (2s and 2p) probability per electron of ionizing one L-shell electron respectively. Using $P_K(b)$ and $\bar{P}_L(b)$, the theoretical ionization cross sections for producing a state having one K-shell and n L-shell vacancies were determined by

$$\sigma_{KL^n} = 2\pi\int_0^y \binom{2}{1} P_K(b)(1-P_K(b)) \binom{8}{n} \bar{P}_L(b)^n (1-\bar{P}_L(b))^{8-n} b\,db. \qquad (5.15)$$

The integration of Eq. (5.15) over impact parameters was accomplished by the Gaussian numerical integration method described in Appendix A. The upper limit of the integral was determined by the K-shell probabilities and was selected such that the K-shell probability at the upper limit was more than a factor of 10^4 smaller than the maximum K-shell probability at that energy. The lower limit of the integral was selected to be zero.

The p_L value for each energy was then calculated from the ionization cross sections by

$$p_L = \frac{1}{8} \sum_{n=1}^{7} n \frac{\sigma_{KL^n}}{\sigma_{tot}}, \qquad (5.16)$$

where σ_{tot} is the sum of the ionization cross sections of all the vacancy configurations.

The results of the BEA and SCA predictions of p_L on the projectile-to-L-shell electron velocity ratio are shown in Fig. 16. Also shown in Fig. 16 are the experimental p_L values from helium and neon ions incident on aluminum. In Fig. 16(a), the low energy neon on aluminum

FIG. 16. Theoretical and experimental dependence of p_L on the velocity ratio.

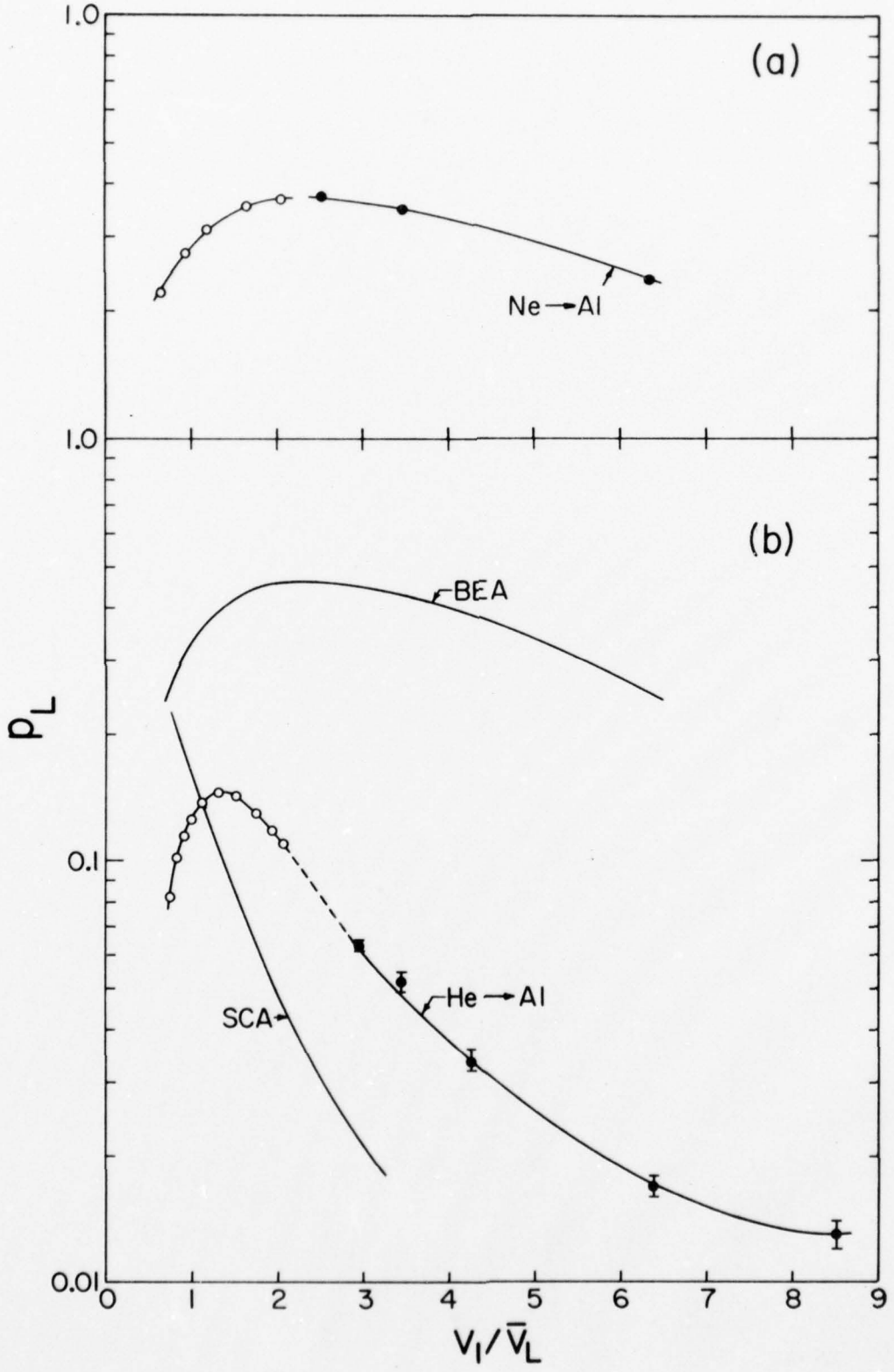
1.0
(a)
Ne → Al
1.0
(b)
BEA
SCA
He → Al
p_L
0.1
0.01
0
1
2
3
4
5
6
7
8
9
$V_l / \bar{V}_L$

data were obtained from a study by Knudson et al.[54] and are indicated by open circles. The low energy helium on aluminum data in Fig. 16(b) indicated by open circles were obtained from a study by Richard et al.[55] The neon p_L values show a very broad maximum centered about a velocity ratio of 2.3 and decrease very slowly with increasing velocity ratio. The experimental helium p_L values in Fig. 16(b), on the other hand, reach a very sharp maximum at a velocity ratio of about 1.25 and decrease much more rapidly than the neon p_L values with increasing velocity ratio. The data for helium on aluminum converge at high velocities with the shakeoff limit observed in photoionization and electron bombardment studies (p_L=0.013).[85] Very good agreement is exhibited here between the two sets of measurements for helium and neon ions on aluminum.

The BEA predictions for helium on aluminum are a factor of 5 to 10 times larger in absolute magnitude than the experimental values. Although the shape of the velocity dependence is not well described by the BEA, a maximum is predicted around a velocity ratio of 2. The BEA results for helium on aluminum are surprisingly similar to the experimental results for neon on aluminum. The SCA predictions more closely represent the slope of the experimental p_L values in the high velocity region, however, they are a factor of about 3 too low. In the low velocity region, greater divergence from the experimental data is seen. The SCA fails to predict the maximum in the region where this feature is found experimentally.

The helium on aluminum combination was used to test the applicability of the BEA and SCA to the description of multiple ionization

because of the low states of ionization resulting from these impacts. These low states of ionization (an average of 1.2 L-shell vacancies for the highest state of ionization in Fig. 16(b)) are not expected to be greatly influenced by variations in the fluorescence yields for different vacancy configurations (as shown in Fig. 13) or by fast rearrangement.

Similar calculations were made for the heavier projectiles but these proved to be meaningless. The BEA and SCA greatly over predicted L-shell ionization to the extent that the probabilities of ionizing one L-shell electron was essentially equal to unity at all energies.

CHAPTER VI

CONCLUSIONS

The results of this study have provided a comprehensive picture of the dependence of the aluminum and silicon Kα x-ray satellite structure on the atomic number and energy of the projectile at high energies. The energies used in this study were above the energy region for maximum L-shell ionization and consequently, decreasing p_L values were observed with increasing projectile energy. The dependence was also observed to flatten with increasing projectile atomic number as the region of the p_L maximum was approached. This flattening is suggestive of a saturation effect in which the x-ray satellite spectra of heavy ions no longer reflect the initial vacancy distribution. The initial vacancy distribution may be altered by L-shell vacancy filling in the highly ionized atom prior to x-ray emission by intra- and interatomic processes. The silicon, silicon monoxide, and silicon dioxide results indicate that fast rearrangement does occur to some extent.

The data from this study were found to be in excellent agreement with the results of previous studies by Richard *et al.*[55] and Knudson *et al.*[54] Together, they provide a very good picture of the dependence of the p_L values on the energy of the projectile for helium on aluminum and neon on aluminum over a broad energy region.

The comparison of the experimental data with theoretical predictions were rather discouraging. The BEA greatly overpredicted the magnitude of the p_L values and failed to accurately predict the shape

of the dependence. The SCA predictions more closely represented the slope of the experimental p_L values at the higher velocities but were too low in magnitude. At the lower energies, greater divergence from the experimental values were observed. The results of the present investigation clearly demonstrate that a much more sophisticated theoretical treatment of multiple inner-shell ionization will be required for a full understanding of the velocity dependence of this process.

REFERENCES

[1]W. K. Roentgen, Ann. Physik der Wurzburg Ges. 64, 1(1895).

[2]J. Chadwick, Phil. Mag. 24, 594(1912).

[3]J. Chadwick, Phil. Mag. 25, 193(1913).

[4]J. Chadwick and A. S. Russell, Proc. Roy. Soc. A 88, 217(1913).

[5]W. L. Bragg, Proc. Roy. Soc. 89, 246(1913).

[6]H. G. Moseley, Phil. Mag. 26, 1024(1913).

[7]H. G. Moseley, Phil. Mag. 27, 703(1914).

[8]J. J. Thomson, Phil. Mag. 28, 620(1914).

[9]M. Siegbahn and W. Stenstrom, Physik Zeits. 17, 48 and 318(1916).

[10]F. K. Richtmyer and R. D. Richtmyer, Phys. Rev. 34, 574(1929).

[11]F. R. Hirsh, Jr., Phys. Rev. 38, 914(1931).

[12]O. R. Ford, Phys. Rev. 41, 577(1932).

[13]C. Gerthsen, Z. Physik 36, 540(1926).

[14]W. M. Coates, Phys. Rev. 46, 542(1934).

[15]H. W. Lewis, B. E. Simmons, and E. Merzbacher, Phys. Rev. 91, 943(1953).

[16]T. Huus and C. Zupancic, Kgl. Dan. Vid. Selsk. Mat. Fys. Medd. 28, No. 1(1953).

[17]G. Wentzel, Ann. d. Physik 66, 437(1921).

[18]G. Wentzel, Zeits. f. Physik 31, 445(1925).

[19]F. K. Richtmyer, J. Frank. Inst. 208, 325(1929).

[20]P. Richard, I. L. Morgan, T. Furuta, and D. Burch, Phys. Rev. Lett. 23, 1009(1969)

[21]D. Burch and P. Richard, Phys. Rev. Lett. 25, 983(1970).

[22]P. H. Mokler, Phys. Rev. Lett. 26, 811(1971).

[23]H. J. Specht, Z. Phys. 185, 301(1965).

[24]P. Richard, T. I. Bonner, T. Furuta, I. L. Morgan, and J. R. Rhodes, Phys. Rev. A 1, 1044(1970).

[25]A. R. Knudson, D. J. Nagel, P. G. Burkhalter, and K. L. Dunning, Phys. Rev. Lett. 26, 1149(1971).

[26]D. Burch, P. Richard, and R. L. Blake, Phys. Rev. Lett. 26, 1355(1971).

[27]D. G. McCrary and P. Richard, Phys. Rev. A 5, 1249(1972).

[28]D. G. McCrary, M. Senglaub, and P. Richard, Phys. Rev. A 6, 263(1972).

[29]F. Herman and S. Skillman, Atomic Structures Calculations(Prentice-Hall, Englewood Cliffs, N. J., 1963).

[30]C. Froese Fischer, Comput. Phys Commun. 1, 157(1969).

[31]W. J. Viegele, D. E. Stevenson, and E. M. Henry, J. Chem. Phys. 50, 5404(1969).

[32]B. B. Ray, Phil. Mag. 8, 772(1929).

[33]R. M. Langer, Phys. Rev. 37, 457(1931).

[34]H. C. Wolfe, Phys. Rev. 43, 221(1933).

[35]C. P. Bhalla, Phys. A 12, 122(1975).

[36]C. P. Bhalla, Phys. Lett. 54A, 249(1975).

[37]R. L. Kauffman, C. W. Woods, K. A. Jamison, and P. Richard, Phys. Lett. 50A, 117(1974).

[38]D. Burch and H. Swanson, Proceedings of the International Conference on Inner-Shell Ionization Phenomena, Atlanta, 1972, Conf.-720404 (USAEC), Vol. 2, p. 1464.

[39]R. L. Watson, T. Chiao, and F. E. Jenson, Phys. Rev. Lett. 35, 254(1975).

[40]R. L. Kauffman, J. H. McGuire, P. Richard, and C. F. Moore, Phys. Rev. A 8, 1233(1973).

[41]A. R. Knudson, P. G. Burkhalter, and D. J. Nagel, Proceedings of the Fifth International Conference on Atomic Collisions, Gatlinburg(1973).

[42]R. L. Kauffman, C. W. Woods, K. A. Jamison, and P. Richard, Phys. Rev. A 11, 872(1975).

[43]R. L. Kauffman, F. Hopkins, C. W. Woods, and P. Richard, Phys. Rev. Lett. 31, 621(1973).

[44]P. Richard, J. Bolger, D. K. Olsen, and C. F. Moore, Phys. Lett. 41A, 269(1972).

[45]P. G. Burkhalter, A. R. Knudson, D. J. Nagel, and K. L. Dunning, Phys. Rev. A 6, 2093(1972).

[46]J. McWherter, D. K. Olsen, H. H. Wolter, and C. F. Moore, Phys. Rev. A 10, 200(1974).

[47]R. L. Watson, A. K. Leeper, B. I. Sonobe, T. Chiao, and F. E. Jenson, Phys. Rev. A 8, 914(1977).

[48]C. F. Moore, M. Senglaub, B. Johnson, and P. Richard, Phys. Lett. 40A, 107(1972).

[49]T. K. Li, R. L. Watson, and J. S. Hansen, Phys. Rev. A 8, 1258(1973).

[50]F. Hopkins, D. O. Elliot, C. P. Bhalla, and P. Richard, Phys. Rev. A 8, 2952(1973).

[51]R. L. Watson, F. E. Jenson, and T. Chiao, Phys. Rev. A 10, 1230(1974).

[52]K. W. Hill, B. L. Doyle, S. M. Shafroth, D. H. Madison, and R. D. Deslattes, Phys. Rev. A 13, 1334(1976).

[53]V. Dutdiewicz, H. Bakhru, and N. Cue, Phys. Rev. A 13, 306(1976).

[54]A. R. Knudson, D. J. Nagel, and P. G. Burkhalter, Phys. Lett. 42A, 69(1972).

[55]P. Richard, R. L. Kauffman, and J. H. McGuire, Phys. Rev. A 8, 1369 (1973).

[56]D. K. Olsen and C. F. Moore, Phys. Rev. Lett. 33, 194(1974).

[57]J. S. Hansen, Phys. Rev. A 8, 822(1973).

[58]J. M. Hansteen, O. M. Johnsen, and L. Kocbach, Atomic and Nucl. Data Tables 15, 305(1975).

[59]M. Gryzinski, Phys. Rev. 138, A336(1965).

[60]J. H. McGuire and P. Richard, Phys. Rev. A 8, 1374(1973).

[61]Naval Research Laboratory, X-ray Optics Branch, Washington, D. C.

[62]C. Rugge, R. L. Watson, and J. B. Wilhelm, Least-squares fitting programs for x-ray pulse height spectra, Lawrence Radiation Laboratory,

Berkeley(unpublished).

[63] R. L. Watson, H. R. Bowman, and S. G. Thompson, Phys. Rev. 162, 1169 (1967).

[64] R. L. Watson and T. K. Li, Nucl. Phys. A 178, 201(1971).

[65] J. A. Bearden, Rev. Mod. Phys. 39, 78(1967).

[66] E. Storm and H. I. Isreal, Nucl. Data A 7, 565(1970).

[67] J. D. Garcia, Phys. Rev. A 1, 280(1970).

[68] L. C. Northcliffe and R. F. Schilling, Nucl. Data Tables A 7, 233 (1970).

[69] T. L. Hardt, Ph.D. dissertation, Texas A&M University, 1975(unpublished).

[70] R. L. Watson, T. Chiao, F. E. Jenson, and B. I. Sonobe, in Beam-Foil Spectroscopy, edited by I. A. Sellin and D. J. Pegg(Plenum, New York, 1976), Vol. 2, p. 567.

[71] A. R. Knudson, P. G. Burkhalter, and D. J. Nagel, Proceedings of the International Conference on Inner-Shell Ionization, Atlanta, 1972, Conf.-720404 (USAEC), Vol. 3, p.1675.

[72] J. A. Bearden and A. F. Burr, Rev. Mod. Phys. 39, 125(1967).

[73] W. Henneberg, Z. Physik 86, 592(1933).

[74] E. Merzbacher and H. W. Lewis, Encyclopedia of Physics, Vol. 34, edited by S. Flugge(Springer-Verlag, Berlin), 166(1958).

[75] M. Gryzinski, Phys. Rev. 138, A105(1965).

[76] L. Vriens, Proc. Phys. Soc. 90, 935(1967).

[77] E. Gerjuoy, Phys. Rev. 148, 54(1965).

[78] J. Bang and J. M. Hansteen, Mat. Fys. Medd. Dan. Vid. Selsk. 31, No. 13 (1959).

[79] N. F. Mott and S. N. Massey, The Theory of Atomic Collisions(Oxford U. P., London), 3rd edition(1965).

[80] G. S. Khandelwal, H. H. Choi, and E. Merzbacher, Atomic Data 1, 103 (1969).

[81] B. H. Choi, E. Merzbacher, and G. S. Khandelwal, Atomic Data 5, 291 (1973).

[82]B. K. Thomas and J. D. Garcia, Phys. Rev. 159, 39(1969).

[83]J. D. Garcia, R. J. Fortner, and T. M. Kavanagh, Rev. Mod. Phys. 45, 111(1973).

[84]L. Kocbach, Report No. 58, Dept. of Physics, Univ. of Bergen, Bergen, Norway, 1973(unpublished).

[85]T. Aberg, Phys. Lett. 26A, 515(1968).

[86]R. L. Watson, A. K. Leeper, and B. I. Sonobe, Nucl. Instr. Meth. 142, 311(1977).

APPENDIX A

GAUSSIAN INTEGRATION

The integral, $\int_A^B f(x)dx$, can be computed by Gauss' formula often expressed by the equations

$$\int_A^B f(x)dx = \int_{-1}^{1} f(z)dz \qquad (A.1)$$

$$= \sum_{i=1}^{n} w_i f(z_i) \qquad (A.2)$$

$$= w_0 f(0) + \sum_{i=1}^{n/2} w_i [f(z_i) + f(-z_i)] \ , \qquad (A.3)$$

where n is the number of interpolation points, w_i are the weights, and z_i are the abscissas. The interval, [A,B], can be transformed to [-1,1]. Let x = cz + d, then,

$$dx = cdz \qquad (A.4)$$

$$A = -c + d \quad \text{when } z=-1, \text{ and} \qquad (A.5)$$

$$B = c + d \quad \text{when } z=1. \qquad (A.6)$$

Combining Eqs. (A.5) and (A.6), the following relations are obtained:

$$c = \frac{B - A}{2} \quad \text{and} \quad d = \frac{A + B}{2} \ .$$

From Eq. (A.4), if dx = cdz, then

$$g(x) = cg(cz + d) \quad \text{and}$$

$$f(z) = cg(cz + d). \tag{A.7}$$

Equations (A.1) to (A.3) then become

$$\int_A^B g(x)dx = \sum_{i=1}^{m} cw_i g(cz + d), \tag{A.8}$$

where m is a factor that determines the number of interpolation points, n.

The n-point Gaussian integration routine listed at the end of this appendix was written to calculate the integral,

$$\sigma_{KL^n} = 2\pi \int_A^B \binom{2}{1} P_K(b)(1-P_K(b)\binom{8}{n}(\overline{P}_L(b))^n(1-\overline{P}_L(b))^{8-n} bdb \ , \tag{A.9}$$

as described in Chapter V. $P_K(b)$ and $\overline{P}_L(b)$ can be any polynomial function up to and including a fifth order polynomial. The number of interpolation points can be selected. The data card formats are as follows:

Card 1 - title card

Columns	Format	Variable	Identity
3-80	A6		Any title or description

Card 2 - coefficients for the equation, $S6x^5 + s5x^4 + S4x^3 + S3x^2 + S2x + S1$

Columns	Format	Variable	Identity
1-10	F10.6	S1	Coefficients
11-20	F10.6	S2	for
21-30	F10.6	S3	$P_K(b)$

Columns	Format	Variable	Identity
31-40	F10.6	S4	
41-50	F10.6	S5	
51-60	F10.6	S6	

Card 3 - coefficients for the equation, $T6x^5 + T5x^4 + T4x^3 + T3x^2 + T2x + T1$

Columns	Format	Variable	Identity
1-10	F10.6	T1	Coefficients
11-20	F10.6	T2	for
21-30	F10.6	T3	
31-40	F10.6	T4	$\overline{P}_L(b)$
41-50	F10.6	T5	
51-60	F10.6	T6	

Card 4 - integral limits and interpolation points

Columns	Format	Variable	Identity
1-10	F10.6	A	Upper limit of integral
11-20	F10.6	B	Lower limit of integral
21-22	I2	m	Factor to determine number of interpolation points

The possible values for m corresponding to the number of interpolation points are as follows:

Values of m	2	3	4	5	6	10	15	20	40
Number of interpolation points, n	1	2	2	3	3	5	8	10	20

The ionization cross sections in the output are not absolute cross sections. The probabilities for ionization used in determining $P_K(b)$ and $\overline{P}_L(b)$ were normalized for use in the polynomial fitting program,

and the normalized functions were subsequently used in the ionization cross section calculations.

```
          $JOB  76133C                BLAKE SONOBE    GAUSSIAN INTEGRATION
          $IBBOX          C Y C L O T R O N       I N S T I T U T E
IBJOB VERSION 5 HAS CONTROL.  (IBSYS VERSION 13)      07/20/76
$IBJOB
$IBFTC MAIN

      DIMENSION TITLE(13)
      COMMON S1,S2,S3,S4,S5,S6
      COMMON T1,T2,T3,T4,T5,T6
    1 IF (EOF(5)) 600,2,600
    2 READ (5,800) NC
      READ (5,100) TITLE
      WRITE (6,200) TITLE
      IF (NC.EQ.2) GO TO 3
      IF (NC.EQ.1) GO TO 4
      WRITE (6,205) NC
      GO TO 600
    3 READ (5,103) S1,S2,S3,S4,S5,S6
      WRITE (6,202) S6,S5,S4
      WRITE (6,204) S3,S2,S1
    4 READ (5,103) T1,T2,T3,T4,T5,T6
      WRITE (6,203) T6,T5,T4
      WRITE (6,204) T3,T2,T1
      READ (5,101) A,B,M
      WRITE (6,201) A,B,M
      CALL GAUSS (A,B,M,SIG,NC)
      GO TO 1
C
C     ......INPUT FORMATS...........
C
  100 FORMAT (2X,13A6)
  101 FORMAT (2F10.6,I2)
  103 FORMAT (6F10.6)
  800 FORMAT (I1)
C
C     .....OUTPUT FORMATS......
C
  200 FORMAT (1H1,10X,13A6)
  201 FORMAT (1H-,10X,35HTHE INPUT VALUES FOR A,B,AND M ARE,3X,F10.6,
     1   3X,F10.6,3X,3HAND,3X,I2)
  202 FORMAT (1H-,10X,29HTHE INPUT FUNCTION FOR FX1 IS,3X,F10.6,5H*X**5,
     1   3H + ,F10.6,5H*X**4,3H + ,F10.6,5H*X**3,2H +)
  203 FORMAT (1H-,10X,29HTHE INPUT FUNCTION FOR FX2 IS,3X,F10.6,5H*X**5,
     1   3H + ,F10.6,5H*X**4,3H + ,F10.6,5H*X**3,2H +)
  204 FORMAT (1H0,15X,F10.6,5H*X**2,3H + ,F10.6,2H*X,3H + ,F10.6)
  205 FORMAT (1H0,10X,4HNC =,I1,2X,19HIS AN INVALID INPUT)
  600 STOP
      END


$IBFTC AA

      SUBROUTINE GAUSS (A,B,M,SIG,NC)
      DIMENSION NPOINT(9), KEY(10), Z(54), WEIGHT(54)
      DATA NPOINT/2,3,4,5,6,10,15,20,40/
      DATA KEY/1,2,4,6,9,12,17,25,35,55/
      DATA NX/9/
```

```
      DATA Z                  /0.57735027 ,0.0        ,0.77459667 ,       ZC001
     1              0.33998104 ,0.86113631 ,0.0        ,0.53846931 ,       ZC002
     2              0.90617985 ,0.23861919 ,0.66120939 ,0.93246951 ,       ZC003
     3              0.14887434 ,0.43339539 ,0.67940957 ,0.86506337 ,       ZC004
     4              0.97390653 ,0.0        ,0.20119409 ,0.39415135 ,       ZC005
     5              0.57097217 ,0.72441773 ,0.84820658 ,0.93727339         ZC006
     6,             0.98799252  ,0.07652652,0.22778585,0.37370609 ,       ZC007
     70.51086700,0.63605368,0.74633191,0.83911697,0.91223443,0.96397193,ZC008
     80.99312860,0.03877242,0.11608408,0.19269758,0.26815219,0.34199409,ZC009
     90.41377920,0.48307580,0.54946713,0.61255389,0.67195668,0.72731826,ZC010
     A0.77830565,0.82461223,0.86595950,0.90209881,0.93281281,0.95791682,ZC011
     B0.97725995,0.99072624,0.99823771/                                 ZC012
      DATA WEIGHT            / 1.0       ,0.88888889 ,0.55555556 ,       WC001
     1              0.65214516 ,0.34785484 ,0.56888889 ,0.47862867 ,       WC002
     2              0.23692688 ,0.46791394 ,0.36076157 ,0.17132449 ,       WC003
     3              0.29552422 ,0.26926672 ,0.21908636 ,0.14945135 ,       WC004
     4              0.06667134 ,0.20257824 ,0.19843148 ,0.18616100 ,       WC005
     5              0.16626921 ,0.13957068 ,0.10715922 ,0.07036605 ,       WC006
     6              0.03075324 ,0.15275339,0.14917299,0.14209611,          WC007
     70.13168864,0.11819453,0.10193012,0.08327674,0.06267205,0.04060143,WC008
     80.01761401,0.07750595,0.07703982,0.07611036,0.07472317,0.07288658,WC009
     90.07061165,0.06791205,0.06480401,0.06130624,0.05743977,0.05322785,WC010
     A0.04869581,0.04387091,0.03878217,0.03346020,0.02793701,0.02224585,WC011
     B0.01642106,0.01049828,0.00452128/                                 WC012
      IF (NC.EQ.1) GO TO 60
      IF (NC.EQ.2) GO TO 50
C
C     IONIZATION CALCULATION OF L L-SHELL VACANCIES
C
   50 DO 10 K=1,9
      L=K-1
C     .....THE FOLLOWING VALUE IS  8 FACTORIAL
      XF8=40320.0
C
C     ....THE FOLLOWING CALCULATES L FACTORIAL  .....
C
      XFL = 1.0
      DO 15 L1=1,L
      C1 = FLOAT(L1)
   15 XFL = XFL*C1
C
C     ....THE FOLLOWING CALCULATES (8-L) FACTORIAL
C
      L8=8-L
      XF8L = 1.0
      DO 20 L2=1,L8
      C2 = FLOAT(L2)
   20 XF8L = XF8L*C2
      DO 1 I = 1,NX
    1 IF (M.EQ.NPOINT(I)) GO TO 2
      SIG=0.0
      WRITE (6,210) M
      RETURN
C
C     .....SET UP INITIAL PARAMETERS .......
C
    2 JFIRST=KEY(I)
      JLAST = KEY(I+1)-1
      C=(B-A)/2.0
      D=(B+A)/2.0
```

```
      SUM=0.0
C
C     ......SUMMATION OF TERMS.....
C
      DO 5 J=JFIRST,JLAST
      IF (Z(J).LE.0.0) SUM = SUM + WEIGHT(J) * (2.*FX1(D) *
     1  (1. -FX1(D))* (XF8/(XF8L*XFL)) * FX2(D)**L*(1.-FX2(D))**(8-L)*D)

    5 IF (Z(J).GT.0.0) SUM = SUM + WEIGHT(J) * ((2.*(FX1(Z(J)*C+D) *
     A    (1.-FX1(Z(J)*C+D))) * (XF8/(XF8L*XFL)) * (FX2(Z(J)*C+D)**L *
     B    (1.-FX2(Z(J)*C+D)) ** (8-L) * (Z(J)*C+D)) + (2.*FX1(-Z(J)*C+D)
     C    * (1.-FX1(-Z(J)*C+D)) * (XF8/(XF8L*XFL)) * FX2(-Z(J)*C+D)
     D    **L * (1.-FX2(-Z(J)*C+D)) ** (8-L) * (-Z(J)*C+D))))


      TWOPI=6.283185
      SIG = TWOPI*C*SUM
   10 WRITE (6,202) L,SIG
      GO TO 70
C
C     ........THIS PORTION PERFORMS A GAUSSIAN INTEGRATION OF .........
C     ........OF ANY POLYNOMIAL UP TO THE FIFTH ORDER...........
C
   60 DO 6 I=1,NX
    6 IF (M.EQ.NPOINT(I)) GO TO 7
      SIG=0.0
      WRITE (6,210) M
  210 FORMAT (1H0,10X,I2,2X,25HIS AN INVALID VALUE FOR M)
      RETURN
C
C     .....SET UP INITIAL PARAMETERS .......
C
    7 JFIRST=KEY(I)
      JLAST = KEY(I+1)-1
      C=(B-A)/2.0
      D=(B+A)/2.0
      SUM=0.0
C
C     ......SUMMATION OF TERMS.....
C
      DO 8 J=JFIRST,JLAST
      IF (Z(J).LE.0.0) SUM = SUM + WEIGHT(J) * FX1(D) * D
    8 IF (Z(J).GT.0.0) SUM = SUM + WEIGHT(J) * ((FX1(Z(J)*C + D) *
     1    (Z(J) * C + D)) + (FX1(-Z(J) * C + D) * (-Z(J) * C + D)))
      SIG = C*SUM
      WRITE (6,205) SIG
  200 FORMAT (1H1,10X,13A6)
  202 FORMAT (1H0,10X,21HTHE CROSS SECTION FOR,2XI1,2X,20HL-SHELL VACANC
     1IES IS,2X,F10.6)
  205 FORMAT (1H0,10X,29HTHE SUM OF THE INTEGRATION IS,F10.6)
   70 RETURN
      END



$IBFTC BB

C     THIS SUBROUTINE DESCRIBES THE K-SHELL PROBABILITY OF IONIZATION
      FUNCTION FX1 (X)
```

```
      COMMON S1,S2,S3,S4,S5,S6
      COMMON T1,T2,T3,T4,T5,T6
      FX1=S6*X**5 + S5*X**4 + S4*X**3 + S3*X**2 + S2*X + S1
      RETURN
      END


$IBFTC CC

C     THIS SUBROUTINE DESCRIBES THE L-SHELL PROBABILITY OF IONIZATION
      FUNCTION FX2 (X)
      COMMON S1,S2,S3,S4,S5,S6
      COMMON T1,T2,T3,T4,T5,T6
      FX2=T6*X**5 + T5*X**4 + T4*X**3 + T3*X**2 + T2*X + T1
      RETURN
      END
 THE FIRST LOCATION NOT USED BY THIS PROGRAM IS 00460.
 THE FIRST LOCATION NOT USED BY THIS PROGRAM IS 01217.
 THE FIRST LOCATION NOT USED BY THIS PROGRAM IS 00115.
 THE FIRST LOCATION NOT USED BY THIS PROGRAM IS 00115.
$DATA



SCA CALCULATION     HE ON AL     V1/VL = 3.0

THE INPUT FUNCTION FOR FX1 IS    -0.      *X**5 +  -0.000641*X**4 +   0.005047*X**3 +
     -0.008975*X**2 +  -0.012925*X +   0.036866

THE INPUT FUNCTION FOR FX2 IS    -0.      *X**5 +  -0.      *X**4 +   0.000475*X**3 +
     -0.003348*X**2 +  -0.000289*X +   0.029544

THE INPUT VALUES FOR A,B,AND M ARE,     0.200000     4.000000   AND   15
THE CROSS SECTION FOR  0  L-SHELL VACANCIES IS    0.419104
THE CROSS SECTION FOR  1  L-SHELL VACANCIES IS    0.072103
THE CROSS SECTION FOR  2  L-SHELL VACANCIES IS    0.006051
THE CROSS SECTION FOR  3  L-SHELL VACANCIES IS    0.000307
THE CROSS SECTION FOR  4  L-SHELL VACANCIES IS    0.000010
THE CROSS SECTION FOR  5  L-SHELL VACANCIES IS    0.000000
THE CROSS SECTION FOR  6  L-SHELL VACANCIES IS    0.000000
THE CROSS SECTION FOR  7  L-SHELL VACANCIES IS    0.000000
THE CROSS SECTION FOR  8  L-SHELL VACANCIES IS    0.000000
```

APPENDIX B

SENSITIVITY

The measurements of the Al and Si Kα x-ray spectra can be used to determine the dependence of the sensitivity of x-ray detection with a crystal spectrometer on the atomic number and energy of the projectile. Sensitivity is of utmost importance in analytical applications of these measurement procedures and in measuring the Kα x-ray spectra to study the satellite dependence on such factors as the chemical environment and the atomic number of the target atom. In analytical applications, Kα x-ray spectral information can be used in quantitative analysis, in the determination of chemical composition, and in measuring the thicknesses of surface layers.[86]

The curves in Fig. 17 give a relative measure of the dependence of the sensitivity of x-ray detection on the atomic number and energy of the projectile and illustrate the importance of proper selection of projectiles and projectile energies for maximum sensitivity. The ratios of the total Al and Si Kα x-ray peak areas to the total background areas (beneath the x-ray peaks) in spectra obtained with He, C, O, and Ne ions ranging in energy from 1 to 10 MeV/amu are shown in Fig. 17. The curves for aluminum and silicon are basically similar. At the lower energies, all the curves exhibit peak to background (P/B) ratios between 5 and 20 which rapidly drop as the projectile energy increases. Between 2.5 and 4.0 MeV/amu, the P/B ratios abruptly change to lower rates of decrease with increasing projectile energy. The rapid drop in the P/B ratios

FIG. 17. The dependence of the peak to background (P/B) ratio for Al and Si Kα x-rays on projectile energy and atomic number.

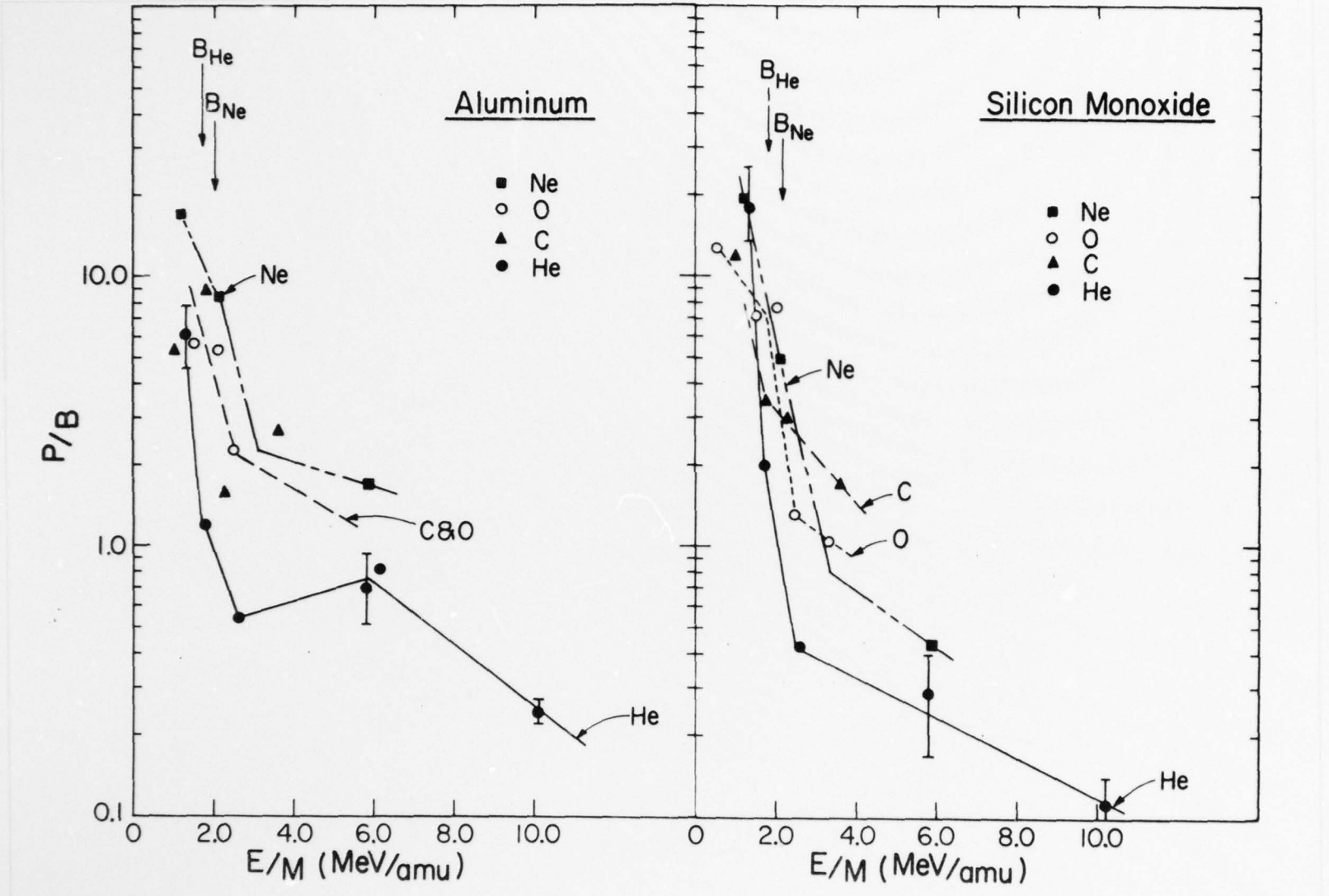
Aluminum
Silicon Monoxide
Ne
O
C
He
B_{He}
B_{Ne}
C&O
P/B
E/M (MeV/amu)
10.0
1.0
0.1
0
2.0
4.0
6.0
8.0
10.0

occurs in the energy region which closely corresponds to the center-of-mass projectile energies necessary to overcome the nuclear Coulomb barriers in aluminum and silicon (shown by the vertical arrows in Fig. 17). This suggests that the majority of the background measured at the higher projectile energies is the result of nuclear reactions. The error bars shown on the helium ion curves in Fig. 17 illustrate the amount of variation of the P/B ratios observed in several different runs. These variations can be caused by factors such as beam spot size and soller slit and crystal alignment, and may well account for the inconsistencies of the carbon on aluminum, helium on aluminum, and oxygen on silicon monoxide curves. The oxygen ion data were obtained from previous measurements made by Watson et al.[47,86]

From Fig. 17, it appears that overall the sensitivity is best with neon ions, however, the sensitivities for Si Kα x-rays are not significantly different for any of the projectiles below approximately 2 MeV/amu. In all cases, the P/B ratios reach their highest values at the lowest energies available in this work (0.5 to 1.5 MeV/amu). This is also the energy region at which the L-shell ionization reaches a maximum (see Fig. 16).

VITA

Blake Isamu Sonobe was born on January 17, 1948 in Honolulu, Hawaii. His parents, Stanley and Elaine Sonobe, currently reside in Belmont, California. He graduated from Samuel F. B. Morse High School, San Diego, California in 1966 and attended the United States Air Force Academy where he graduated in 1970 with a Bachelor of Science degree in Chemistry. Mr. Sonobe was commissioned an officer in the United States Air Force upon graduation and was assigned to Eglin Air Force Base where he served as a project engineer in the development of non-nuclear munitions, as a chemist in explosives development, and as the chief of the Explosive Dynamics Testing Laboratory.

During his degree program under the direction of Dr. Rand L. Watson, Mr. Sonobe was supported by the Air Force Institute of Technology. He is a member of the American Chemical Society.

Mr. Sonobe resides at Quarters 6301-I, USAF Academy, Colorado with his wife, Janie, and daughter, Abigail. He is assigned as an instructor in the Department of Chemistry and Biological Sciences at the United States Air Force Academy.